CHAPTER 7

Syntheses, Crystal structures, Lone Pair Functionality and Electrospray Ionization Mass Spectral Properties of Trinuclear, Dimer of Trinuclear and Trinuclear-Based One-Dimensional Systems of Copper(II) and Lead(II)

7.1. Introduction

Self-assembled supramolecular structures are of great interest due to their aesthetic beauty and possibility of application as functional materials.[1–27] Coordination polymers[3–7,11,14,15–27] belong to a class of supramolecules where individual building blocks are interlinked by bridging organic or inorganic ligands including di and tri carboxylates[6,7,15–18] and dicyanamide.[17,19–27]

Single-compartmental and double-compartmental Schiff base ligands obtained on condensing salicylaldehyde / 2-hydroxyacetophenone / 3-methoxysalicylaldehyde / 3-ethosysalicylaldehyde and a diamine occupy a dominating position in coordination chemistry.[3,27–61] Several mono/[3,39,40,47–49] di/[3,29,30,32–34,36,39–41,44–47,53,54,60,61] oligonuclear [3,39,40,47] and polymeric metal complexes[3,27,39,40,47] have been reported from these ligands. These ligands are suitable to derive heteronuclear complexes.[3,27–47,50–61] Most of the heteronuclear complexes from this family contain Cu^{II}/Ni^{II} in the $N(imine)_2O(phenoxo)_2$ compartment.[3,27–47,50–61] The approach of synthesizing heteronuclear systems is the isolation of a mononuclear Cu^{II}/Ni^{II} complex, which is then used as a metallo-ligand and treated with a second metal ion to derive heteronuclear compounds. A number of the derived heteronuclear complexes have displayed interesting structural[35,39,40,47,50–61] and magnetic properties. [28,29,34,35,38,39,40,42,43,46,47,56,57,59,60] Most of these Cu^{II}/Ni^{II}–second metal ion complexes are dinuclear $Cu^{II}M^{I/II}/Ni^{II}M^{I/II}$[3,29,30,32–34,36,39–41,44–47,53,54,60,61] and trinuclear $Cu^{II}M^{I/II}Cu^{II}/Ni^{II}M^{I/II}Ni^{II}$ [3,28,31,37,39–45,53,55] (M = Zn, Cu, Ni, Co, Mn, Fe, Li, Na, K, Rb, Cs, Mg, Ca, Sr, Pb, Bi, Ln, $U^{VI}O_2$, and Ag etc.). The other types of systems include some cocrystals of dinuclear $Cu^{II}M^{I/II}/Ni^{II}M^{I/II}$ and mononuclear Cu^{II}/Ni^{II} moieties [43,47,50,51,54,55,56,58,59,61] and rare examples of metal (M^{II}) centered $M^{II}Cu^{II}_3$ stars (M = Zn, Cu, Ni, Mn, and Cd).[27,35]

Notably, some complexes from above mentioned ligands are also known where bridging ligands have been used as spacers to interlink the di/trinuclear nodes to generate coordination polymers.[17,22–27] However, heteronuclear compounds containing copper(II)/nickel(II)/zinc(II) and lead(II) from the above class of ligands [3,53–55,61–71] were not previously treated to assemble by bridging inorganic/organic ligands. One aim of this investigation is to explore the structural aspects of copper(II)–lead(II) compounds from above mentioned class of Schiff base ligands and inorganic/organic bridging ligands. It

may be mentioned also that Pb^{II} compounds deserve importance also from the perspective of exploration of its lone pair functionality and accompanied distortion of coordination environment.[72–76]

Varieties of heterometallic compounds are known from the above mentioned Schiff base ligands, revealing structural diversity as the function of metal–metal combination and particular Schiff base ligand.[27,35,50–61] However, electrospray ionization mass spectral (ESI-MS) studies of only few of them have been carried out previously.[33,35,38,58,61,67,69] As this spectral technique deals with stabilization of ionic species in gaseous state, it may be interesting to explore the nature of ionic gaseous species arising from heterometallic compounds derived from Schiff base ligands.

With the aims to explore the structural aspects, lone pair functionality of lead(II) and gaseous ionic species, we are reporting herein the syntheses, crystal structures and electrospray ionization mass spectral study of four heteronuclear compounds of composition $[(Cu^{II}L^{8})_2Pb^{II}(ClO_4)_2]$ (**31**), $[(Cu^{II}L^{6})_2Pb^{II}(NO_3)_2]$ (**32**), $[\{(Cu^{II}L^{6})_2Pb^{II}\}_2(\mu$-adipate$)](ClO_4)_2{\cdot}2H_2O$ (**33**), and $[(Cu^{II}L^{6})_2Pb^{II}(\mu_{1,5}$-dicyanamide$)_2]_n$ (**34**), where H_2L^{8}, H_2L^{6} are the [1+2] condensation products of 1,3-diaminopropane and 2,2-dimethyl-1,3-diaminopropane respectively with salicylaldehyde (Chart 7.1.).

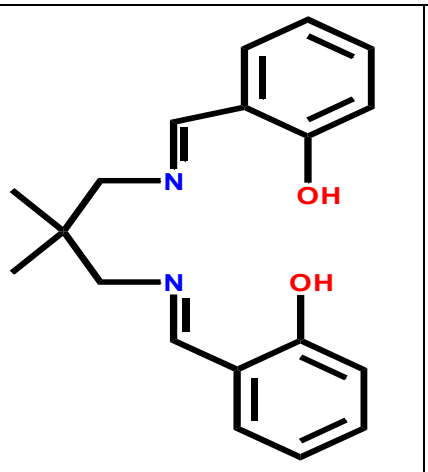

Chart 7.1. Chemical Structure of the Ligand $\mathbf{H_2L^6}$ and $\mathbf{H_2L^8}$.

7.2. Experimental Section

7.2.1. Materials and Physical Measurements

All the reagents and solvents were purchased from commercial sources and used as received. The ligands H_2L^8,[77] H_2L^6,[78] as well as the mononuclear compounds $[Cu^{II}L^8(H_2O)]$[79] and $[Cu^{II}L^6]$[80] were synthesized by reported procedures. Elemental (C, H, and N) analyses were performed on a Perkin-Elmer 2400 II analyzer. FT-IR spectra were recorded in the region 400–4000 cm^{-1} on a Bruker-Optics Alpha-T spectrophotometer with samples as KBr disks. UV-Visible studies were performed with a Shimadzu UV-3600 spectrophotometer. The electrospray ionization mass spectra were recorded on a Waters Xevo G2 QTOF Mass Spectrometer. Molar conductivity was measured at 25º C with a Systronics conductivity bridge.

7.2.2. Syntheses

$[(Cu^{II}L^8)_2Pb^{II}(ClO_4)_2]$ (31) and $[(Cu^{II}L^6)_2Pb^{II}(NO_3)_2]$ (32). These two compounds were prepared by following similar procedures: To a methanol suspension (10 mL) of the corresponding mononuclear compound, $[Cu^{II}L^8(H_2O)]$ (for **31**; 0.050 g, 0.14 mmol)/$[Cu^{II}L^6]$ (for **32**; 0.050 g, 0.13 mmol), solid lead(II) perchlorate trihydrate (for **31**; 0.063g, 0.14 mmol)/lead(II) nitrate (for **32**; 0.044 g, 0.13 mmol) was added with stirring. The resulted green solution was filtered after a few minutes and the filtrate was kept at room temperature for slow evaporation. Green crystalline compounds containing diffraction quality single crystals that deposited after 2–3 days were collected by filtration and washed with MeOH.

$[\{(Cu^{II}L^6)_2Pb^{II}\}_2(\mu\text{-adipate})](ClO_4)_2\cdot 2H_2O$ (33) and $[(Cu^{II}L^6)_2Pb^{II}(\mu_{1,5}\text{-dicyanamide})_2]_n$ (34). These two compounds were prepared by following similar procedures: To a stirred suspension of $[Cu^{II}L^6]$ (0.050 g, 0.13 mmol) in MeOH (10 mL), was dropwise added a MeOH solution (5 mL) of lead(II)perchlorate trihydrate (0.062 g, 0.13 mmol). After a few minutes an aqueous solution of adipic acid (for **33**; 0.039 g, 0.27 mmol)/sodium dicyanamide (for **34**; 0.048 g, 0.54 mmol) was added to the green solution. Stirring was continued for another 30 min and then the solution was filtered.

The clear green filtrate was kept under ambient temperature for slow evaporation. Diffraction quality green single crystals that were deposited after few days was collected by filtration and washed with MeOH.

7.2.3. Analytical and FT-IR Data

For **31**: Anal. Calcd for $C_{34}H_{32}N_4O_{12}Cl_2Cu_2Pb$: C, 37.33; H, 2.95; N, 5.12%. Found: C, 37.30; H, 2.97; N, 5.11%. FT-IR on KBr (cm^{-1}): ν(C=N), 1614 s; ν(ClO_4), 1121 s, 1108 s, 625 w and 617 w.

For **32**: Anal. Calcd for $C_{38}H_{40}N_6O_{10}Cu_2Pb$: C, 42.45; H, 3.75; N, 7.82%. Found: C, 42.47; H, 3.74; N, 7.81%. FT-IR on KBr (cm^{-1}): ν(C=N), 1617 s; ν(nitrate), 1424 m and 1270 s.

For **33**: Anal. Calcd for $C_{82}H_{92}N_8O_{22}Cl_2Cu_4Pb_2$: C, 43.17; H, 4.06; N, 4.91%. Found: C, 43.51; H, 4.02; N, 4.96%. FT-IR on KBr (cm^{-1}): ν(H_2O), 3423 m; ν(C=N), 1612 vs; $\nu_{as}(CO_2)$, 1550 s; $\nu_s(CO_2)$, 1471 s; ν(ClO_4), 1091 s and 621 w.

For **34**: Anal. Calcd for $C_{42}H_{40}N_{10}O_4Cu_2Pb$: C, 46.57; H, 3.72; N, 12.93%. Found: C, 46.59; H, 3.70; N, 12.95%. FT-IR on KBr (cm^{-1}): ν(C≡N), 2253 m, 2208 m and 2136 s; ν(C=N), 1620 vs.

7.2.4. Crystal Structure Determination of 31–34

The crystallographic data for the four compounds are summarized in Table 7.1. Diffraction data of these four compounds were collected on a Bruker-APEX II CCD diffractometer at 296 K using graphite-monochromated Mo Kα radiation (λ = 0.71073 Å). For data processing and absorption correction the packages SAINT[81]and SADABS [81] were used. The structures were solved by direct and Fourier methods and refined by full-matrix least-squares based on F^2 using SHELXTL[82] and SHELXL-97 packages.[83]

During the development of the structures, it became apparent that a few atoms in **31** and **33** were each disordered over two sites. These disordered atoms are as follows:

O5 of one perchlorate and O9, O10, O11, and O12 of the second perchlorate moiety in **31**, C40 and C41 of the bridging adipate and O7, O8, O9, and O10 of the perchlorate moiety in **33**. The disorders were fixed allowing each individual atom to refine freely and the final occupancy parameters were set as: 0.80/0.20 for C40A/C40B and C41A/C41B in **33**, 0.65/0.35 for O7A/O7B, O8A/O8B, O9A/O9B, and O12A/O12B in **33**, 0.55/0.45 for O5A/O5B in **31** and 0.50/0.50 for O9A/O9B, O10A/O10B, O11A/O11B, and O12A/O12B in **31**.

The following hydrogen atoms could not be located from Fourier difference maps: four hydrogen atoms linked with each of the two solvated water molecules in **33**. All other hydrogen atoms in the four compounds were inserted on geometrically calculated positions with fixed thermal parameters and were refined isotropically, while all the nonhydrogen atoms were refined anisotropically. The final least-squares refinements (R_1) based on $I > 2\sigma(I)$ converged to 0.0349, 0.0366, 0.0415, and 0.0212 for **31**–**34**, respectively.

Table 7.1. Crystallographic Data for **31**–**34**.

	31	**32**	**33**	**34**
empirical formula	$C_{34}H_{32}N_4O_{12}Cl_2Cu_2Pb$	$C_{38}H_{40}N_6O_{10}Cu_2Pb$	$C_{82}H_{88}N_8O_{22}Cl_2Cu_4Pb_2$	$C_{42}H_{40}N_{10}O_4Cu_2Pb$
fw	1093.81	1075.03	2277.04	1083.11
crystal system	triclinic	monoclinic	triclinic	monoclinic
space group	$P\bar{1}$	$C2/c$	$P\bar{1}$	$C2/c$
a (Å)	10.8506(7)	17.4849(10)	11.4997(7)	21.926(2)
b (Å)	11.5393(7)	13.4388(7)	13.4117(9)	9.9192(10)
c (Å)	14.6961(9)	17.2783(9)	14.6949(9)	20.926(3)
α (deg)	89.745(2)	90.00	100.087(3)	90.00
β (deg)	81.308(3)	109.750(2)	105.150(2)	117.329(3)
γ (deg)	89.520(3)	90.00	96.567(3)	90.00
V (Å^3)	1818.9(2)	3821.2(4)	2123.0(2)	4043.2(8)
Z	2	4	1	4
ρ_{calcd} (g cm^{-3})	1.997	1.869	1.781	1.779
μ (mm^{-1})	5.992	5.565	5.075	5.253
T (K)	296(2)	296(2)	296(2)	296(2)
F (000)	1068	2120	1126	2136
2θ (deg)	2.80–55.00	3.92–68.50	2.94–53.00	4.18–53.00
Index ranges	$-13 \le h \le 14$	$-27 \le h \le 27$	$-14 \le h \le 14$	$-27 \le h \le 26$
	$-14 \le k \le 14$	$-20 \le k \le 21$	$-16 \le k \le 16$	$-12 \le k \le 12$
	$-19 \le l \le 19$	$-27 \le l \le 24$	$-18 \le l \le 18$	$-26 \le l \le 25$
Reflections collected	26505	30423	29531	23843
Independent reflections (R_{int})	8179(0.0350)	7867(0.0523)	8668(0.0433)	4144(0.0367)
Parameters refined	535	260	563	269
Goodness-of-fit on F^2	1.012	0.926	1.055	1.026
R_1[a], wR_2[b] ($I > 2\sigma(I)$)	0.0349, 0.0947	0.0366, 0.0711	0.0415, 0.1011	0.0212,0.0473
R_1[a], wR_2[b] (for all data)	0.0487, 0.1116	0.0838, 0.0848	0.0572, 0.1099	0.0250,0.0486

[a] $R_1 = [\sum||F_o| - |F_c||/\sum|F_o|]$. [b] $wR_2 = [\sum w(F_o^2 - F_c^2)^2/\sum wF_o^4]^{1/2}$.

7.3. Results and Discussion

7.3.1. Syntheses and Characterization of $[(Cu^{II}L^8)_2Pb^{II}(ClO_4)_2]$ (31), $[(Cu^{II}L^6)_2Pb^{II}(NO_3)_2]$ (32), $[\{(Cu^{II}L^6)_2Pb^{II}\}_2(\mu\text{-adipate})](ClO_4)_2\cdot 2H_2O$ (33), and $[(Cu^{II}L^6)_2Pb^{II}(\mu_{1,5}\text{-dicyanamide})_2]_n$ (34)

The four complexes, (**31**–**34**) were prepared either by the reaction of the metallo-ligand $[Cu^{II}L^8(H_2O)]/[Cu^{II}L^6]$ with $Pb(ClO_4)_2\cdot 3H_2O$ / $Pb(NO_3)_2$ in 1:1 ratio (for **31** and **32** respectively) or by reaction of the metallo-ligand $[Cu^{II}L^6]$ with $Pb(ClO_4)_2\cdot 3H_2O$ and adipic acid (for **33**) / sodium dicyanamide (for **34**) in 1:1:2 (for **33**) /1:1:4 (for **34**) ratio. Although copper(II) metallo-ligands and Pb^{II} salts were mixed in 1:1 ratio, the

heteronuclear products **31**–**34** consist of trinuclear $Cu^{II}Pb^{II}Cu^{II}$ moieties, i.e., the product have Cu^{II}:Pb^{II} ratio of 2:1. Notably the change of the ratio of the reactants (Cu^{II} and Pb^{II}) does not affect on the composition of the compounds, indicating the specificity of the stabilization of trinuclear $Cu^{II}Pb^{II}Cu^{II}$ cores in these two ligand systems, even in the presence of an auxiliary organic (adipate) or inorganic (dicyanamide) bridging ligand.

The characteristic C=N stretching frequency is observed as a strong band in the range 1612–1620 cm^{-1} for all the complexes **31**–**34**. One strong and two medium intensity bands appear at 2136, 2208, and 2253 cm^{-1} respectively, for compound **34** which are characteristics of the dicynamide ligand (C≡N). Presence of water molecule in compound **33** is evident by the appearance of a band of medium intensity at 3423 cm^{-1}. Carboxylate stretching frequencies due to the asymmetric and symmetric vibration modes, present in compound **33** arise at 1550 and 1471 cm^{-1}, respectively. The presence of nitrate in **32** is evident by the presence of two (one medium and one strong intensity) bands respectively, at 1424 and 1270 cm^{-1} respectively.

In principle, the nature of perchlorate (noncoordinated / monodentate / bidentate chelating) should be rationalized from the IR data. Noncoordinated (T_d), monodentate (C_{3V}) and bidentate chelating (C_{2V}) perchlorate should exhibit two (T_2, around 1100 cm^{-1}; T_2, around 620 cm^{-1}), four (A_1+E; A_1+E) and six (A_1+B_1+B_2; A_1+B_1+B_2) signals[84] However, while this happens for simpler systems where ligand environment has no absorption in the concerned regions, the IR pattern may be complicated to rationalize for systems where ligand environment has absorptions in the concerned regions. The parts of the FT-IR spectra of $[(Cu^{II}L^8)_2Pb^{II}(ClO_4)_2]$ (**31**) and the corresponding Cu^{II} metallo-ligand $[Cu^{II}L^8(H_2O)]$ are compared in Figure 7.1, while the parts of the FT-IR spectra of $[\{(Cu^{II}L^6)_2Pb^{II}\}_2(\mu\text{-adipate})](ClO_4)_2{\cdot}2H_2O$ (**33**) and the corresponding Cu^{II} metallo-ligand $[Cu^{II}L^6]$ are compared in Figure 7.2, revealing that ligand environments in both the cases have absorption in the regions of the absorptions of perchlorate. Albeit, as compared in Figure 7.3, the higher energy absorption of perchlorate in **31** is clearly split at two positions (at 1121 and 1108 cm^{-1}), while that (centered at 1091 cm^{-1}) in **33** should not be considered as a split band (rather, it is zigzag throughout). Regarding the lower energy band, as also compared in Figure 7.4, the band for **31** at 625 cm^{-1} is clearly accompanied with a hump at 617 cm^{-1}, while such split signature is not observed in the case of **33** for

which it is clearly a single absorption at 621 cm^{-1}. While the perchlorate moiety (ies) in both the cases is/are monodentate, such difference should not be observed. However, notably, the perchlorate moiety in **33** is semicoordinated rather than coordinated to Cu^{II} with a long Cu^{II}–O(perchlorate) distance of 2.765 Å (*vide infra*) and so it retains the IR characteristics of an anionic perchlorate. In contrast, the two perchlorate moieties are clearly monodentate to lead(II) in **31** (*vide infra*), revealing the IR characteristics of monodentate perchlorate.

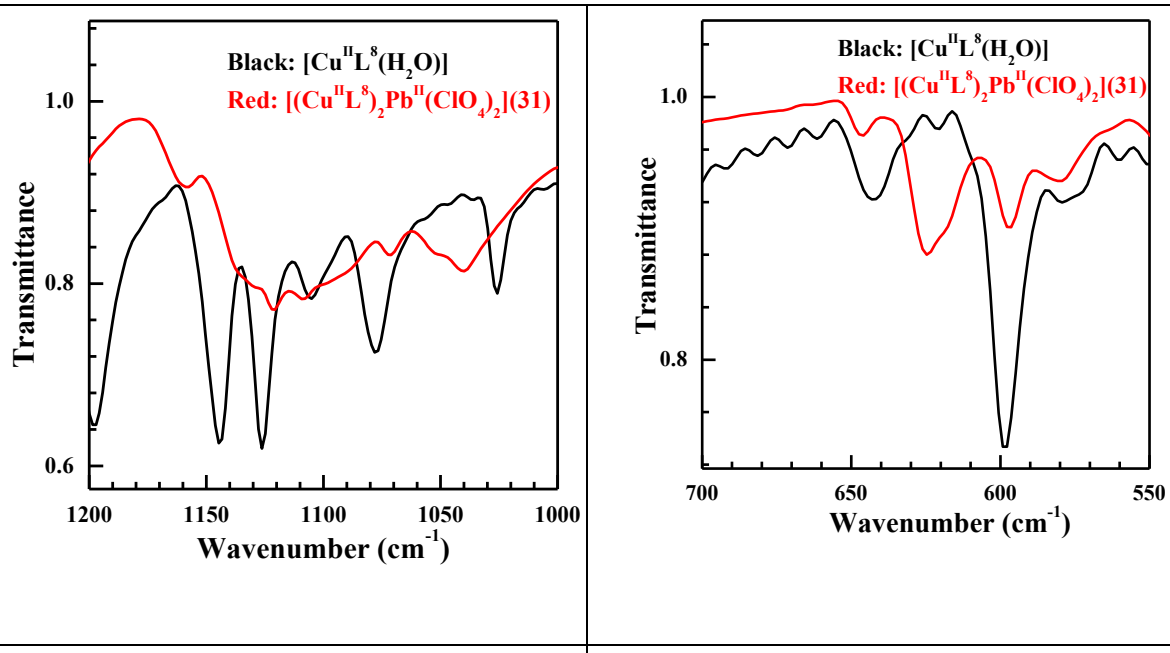

A **B**

Figure 7.1. Comparison of the parts of the FT-IR spectra of $[(Cu^{II}L^{8})_2Pb^{II}(ClO_4)_2]$ (**31**) and corresponding mononuclear Cu^{II} meatllo-ligand $[Cu^{II}L^{8}(H_2O)]$; **A**: in the region 1200–1000 cm^{-1} and **B**: in the region 700–550 cm^{-1}.

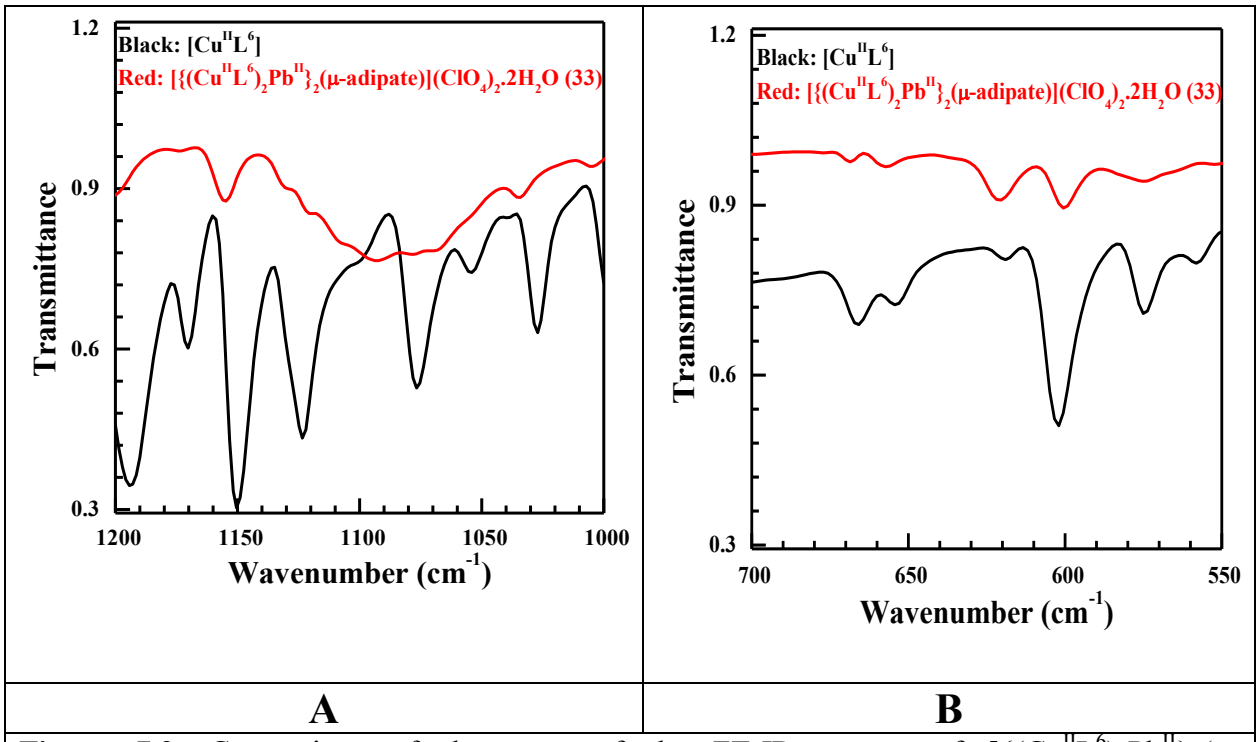

Figure 7.2. Comparison of the parts of the FT-IR spectra of $[\{(Cu^{II}L^{6})_2Pb^{II}\}_2(\mu\text{-adipate})](ClO_4)_2\cdot 2H_2O$ (**33**) and corresponding mononuclear Cu^{II} meatllo-ligand $[Cu^{II}L^{6}]$; **A**: in the region 1200–1000 cm^{-1} and **B**: in the region 700–550 cm^{-1}.

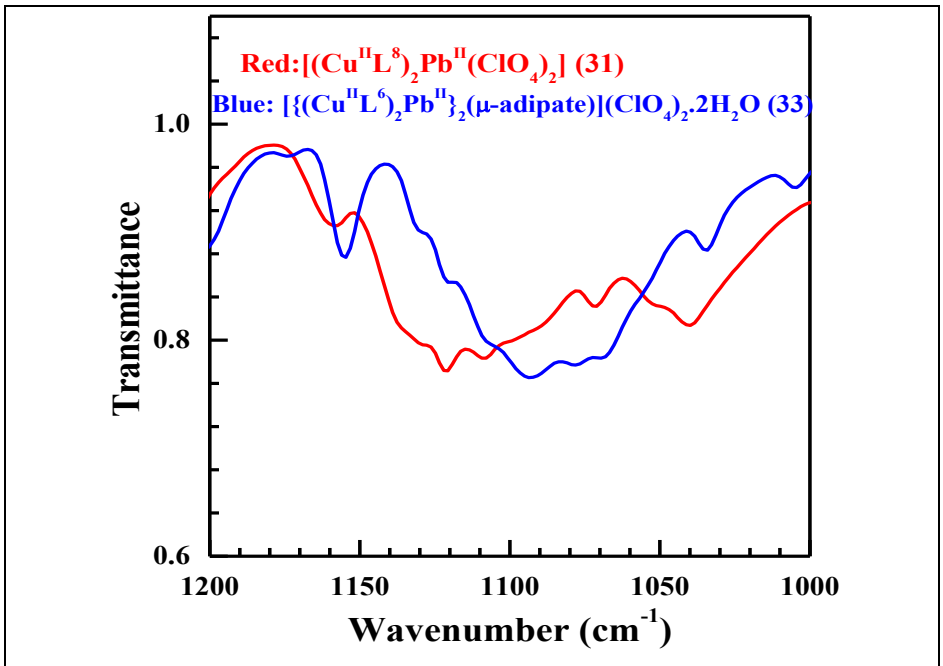

Figure 7.3. Comparison of the parts of the FT-IR spectra of $[(Cu^{II}L^{8})_2Pb^{II}(ClO_4)_2]$ (**31**) and $[\{(Cu^{II}L^{6})_2Pb^{II}\}_2(\mu\text{-adipate})](ClO_4)_2\cdot 2H_2O$ (**33**) in the region 1200–1000 cm^{-1}.

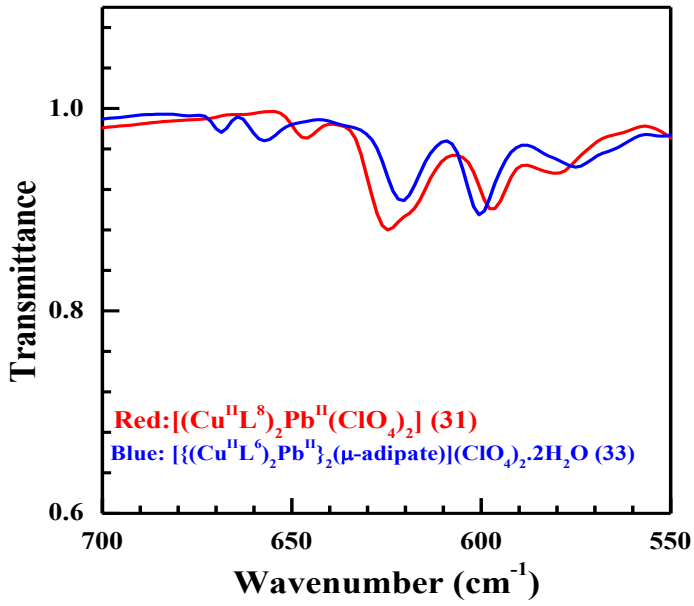

Figure 7.4. Comparison of the parts of the FT-IR spectra of $[(Cu^{II}L^{8})_2Pb^{II}(ClO_4)_2]$ (**31**) and $[\{(Cu^{II}L^{6})_2Pb^{II}\}_2(\mu\text{-adipate})](ClO_4)_2{\cdot}2H_2O$ (**33**) in the region in the region 700–550 cm^{-1}.

To check the nature of composition in solution, we have measured molar conductance of complexes **31**–**34**, with 10^{-3} (M) solutions in MeCN. The values are 200, 32, 210, and 123 Ω^{-1} M^{-1} cm^{-1} L for **31**–**34**, respectively. These indicates[85] that: (i) $[(Cu^{II}L^{8})_2Pb^{II}(ClO_4)_2]$ (**31**) behaves as a 1:2 electrolyte and so it is evident that both the coordinated perchlorate moieties are replaced by solvent molecules; (ii) $[(Cu^{II}L^{6})_2Pb^{II}(NO_3)_2]$ (**32**) is a nonelectrolyte, i.e., it retains its solid state composition in solution; (iii) $[\{(Cu^{II}L^{6})_2Pb^{II}\}_2(\mu\text{-adipate})](ClO_4)_2{\cdot}2H_2O$ (**33**) is a 1:2 electrolyte, i.e., it retains its solid state composition in solution; (iv) $[(Cu^{II}L^{6})_2Pb^{II}(\mu_{1,5}\text{-dicyanamide})_2]_n$ (**34**) behaves as a 1:1 etectrolyte, i.e., the coordination polymer is fragmented in solution and most probably the cationic part in solution is a trinuclear $Cu^{II}Pb^{II}Cu^{II}$ core with one coordinated dicyanamide while the anionic part is one dicyanamide.

The d−d band position (in MeCN) of copper(II) center in **31**–**34**, and the corresponding mononuclear copper(II) compounds appears in the range 600–618 nm with variable intensity: $[Cu^{II}L^{8}(H_2O)]$, 605 nm (ε = 173 $M^{-1}cm^{-1}$); (**31**), 618 nm (ε = 210 $M^{-1}cm^{-1}$); $[Cu^{II}L^{6}]$, 605 nm (ε = 220 $M^{-1}cm^{-1}$); (**32**), 600 nm (ε = 100 $M^{-1}cm^{-1}$); (**33**), 602 nm (ε= 694 $M^{-1}cm^{-1}$), and (**34**), 601 nm (ε= 304 $M^{-1}cm^{-1}$). As already mentioned in the

preceding paragraph, the coordination polymer **34** is fragmented in solution, as also the complex **31**. So, UV-Vis data of **31** and **34** originate from the corresponding fragments in solution.

7.3.2. Description of Structures of 31–34

Crystal structures of **31**–**34** are shown in Figure 7.5 (for **31**), Figure 7.6 (for **32**), Figure 7.7 (for **33**), and Figure 7.8 and Figure7.9 (for **34**). The structures reveal that **31** and **32** are trinuclerar $Cu^{II}Pb^{II}Cu^{II}$ compounds, **33** is a dimer of two trinuclear $Cu^{II}Pb^{II}Cu^{II}$ moieties and **34** is a trinuclear ($Cu^{II}Pb^{II}Cu^{II}$) based one-dimensional coordination polymer. In the trinuclear $Cu^{II}Pb^{II}Cu^{II}$ units of all these compounds **31**–**34**, one Pb^{II} resides in between two $[Cu^{II}L^{8}]$ (for **31**) or $[Cu^{II}L^{6}]$ (for **32**–**34**) moieties. Each Cu^{II} center, obviously, resides in the corresponding $N(imine)_2O(phenoxo)_2$ compartment, i.e., each Cu^{II} center is coordinated to the two imine nitrogen atoms and two phenoxo oxygen atoms of one $[L^{8}]^{2-}/[L^{6}]^{2-}$. The Pb^{II} center in each trinuclear unit is coordinated to the two phenoxo oxygen atoms of each of the two $[Cu^{II}L^{8}]$/ $[Cu^{II}L^{6}]$ units, i.e., copper(II) and lead(II) for the two $Cu^{II}Pb^{II}$ pairs are diphenoxo-bridged. The lead(II) center is additionally coordinated to two oxygen atoms of two terminal perchlorates in **31**, four oxygen atoms of two chelating nitrates in **32**, two carboxylate oxygen atoms of a bridging adipate in **33** and two nitrile nitrogen atoms of two $\mu_{1,5}$-bridging dicyanamides in **34**. The two carboxylate oxygen atoms of the second carboxylate moiety of the adipate ligand in **33**, chelates a second Pb^{II} center of a second $Cu^{II}Pb^{II}Cu^{II}$ unit, forming the hexanuclear (dimer of trinuclear) $(Cu^{II}Pb^{II}Cu^{II})_2$ compound **33**. The two second nitrile nitrogen atoms of the two $\mu_{1,5}$-bridging dicyanamides (one end of each of which is coordinated to the Pb^{II} center of one $Cu^{II}Pb^{II}Cu^{II}$ unit) in **34**, are linked to two copper(II) centers of another trinuclear $Cu^{II}Pb^{II}Cu^{II}$ moiety, and such interlinking of the $Cu^{II}Pb^{II}Cu^{II}$ units by bridging dicyanamides is propagated along the crystallographic *b* axis to generate a one-dimensional coordination polymer.

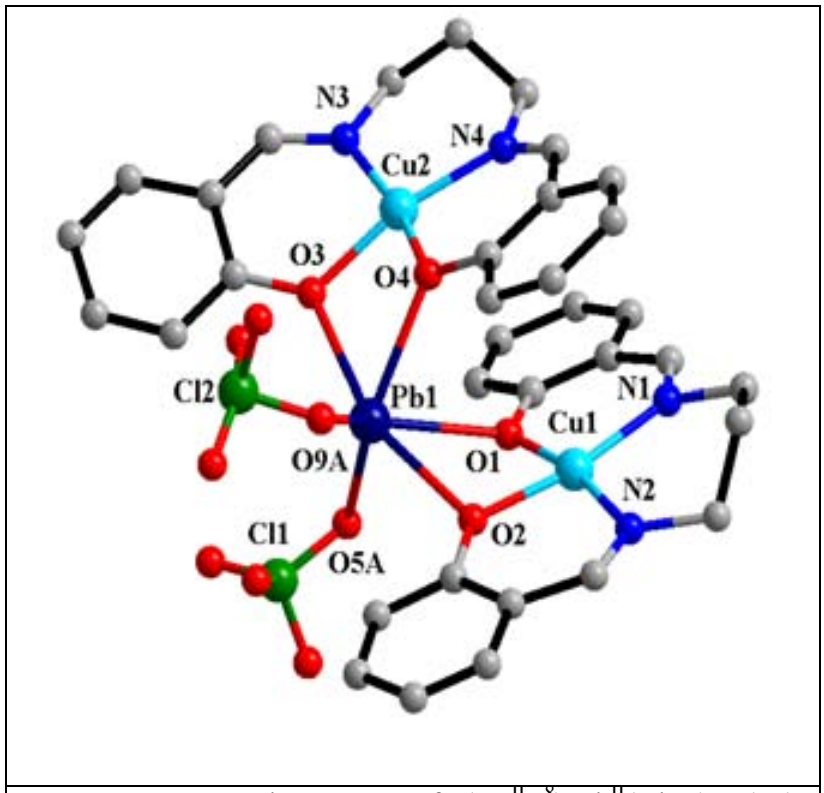

Figure 7.5. Crystal structure of $[(Cu^{II}L^{8})_2Pb^{II}(ClO_4)_2]$ (**31**). All the hydrogen atoms are omitted for clarity.

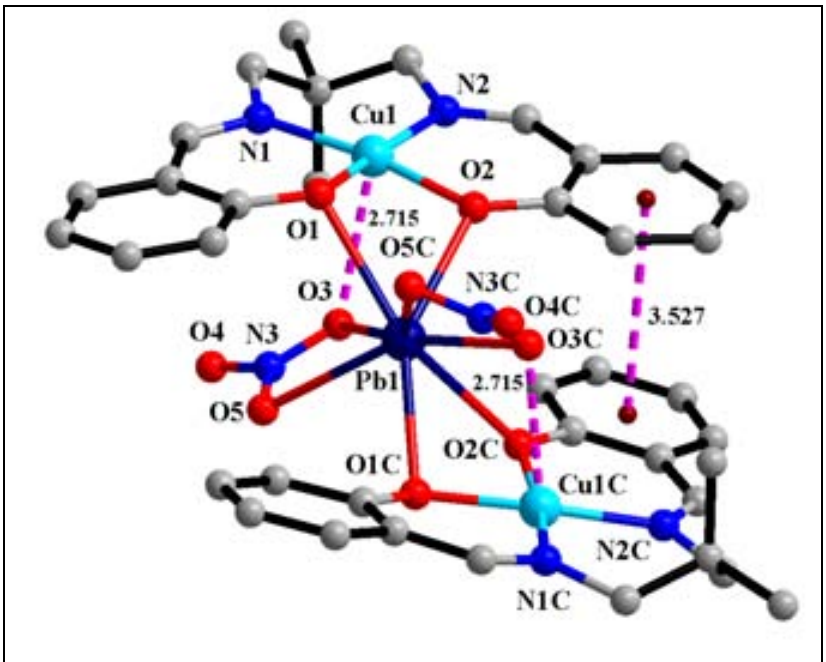

Figure 7.6. Crystal structure of $[(Cu^{II}L^{6})_2Pb^{II}(NO_3)_2]$ (**32**). All the hydrogen atoms are omitted for clarity. Symmetry: C, –x, y, 0.5–z. Bond lengths are shown in Å.

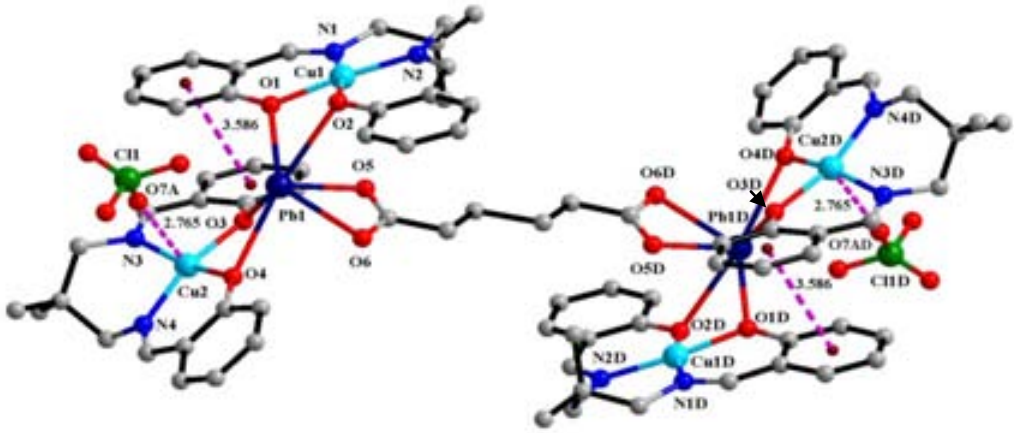

Figure 7.7. Crystal structure of $[\{(Cu^{II}L^{6})_2Pb^{II}\}_2(\mu\text{-adipate})](ClO_4)_2{\cdot}2H_2O$ (**33**). All the hydrogen atoms and the solvated water molecule are omitted for clarity. Symmetry: D, 2–x, 1–y, 2–z. Bond lengths are shown in Å.

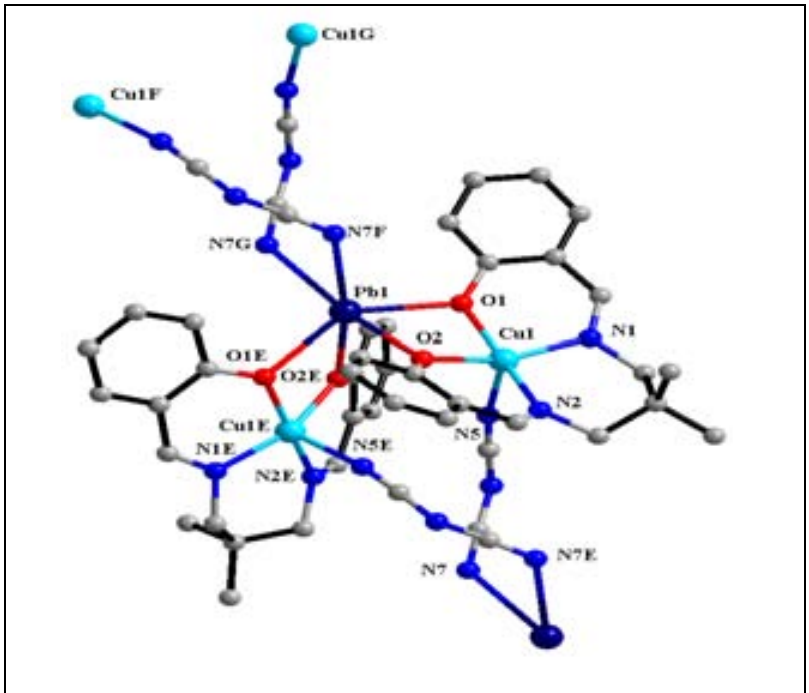

Figure 7.8. Crystal structure of $[(Cu^{II}L^{6})_2Pb^{II}(\mu_{1,5}\text{-dicyanamide})_2]_n$ (**34**), showing the coordination environment of the metal ions and the pattern of interlinking of the $Cu^{II}Pb^{II}Cu^{II}$ units by dicyanamides. All the hydrogen atoms are omitted for clarity. Symmetry: E, –x, y, 0.5–z; F, –*x*, –1+y, 0.5–z; G, x, –1+y, z.

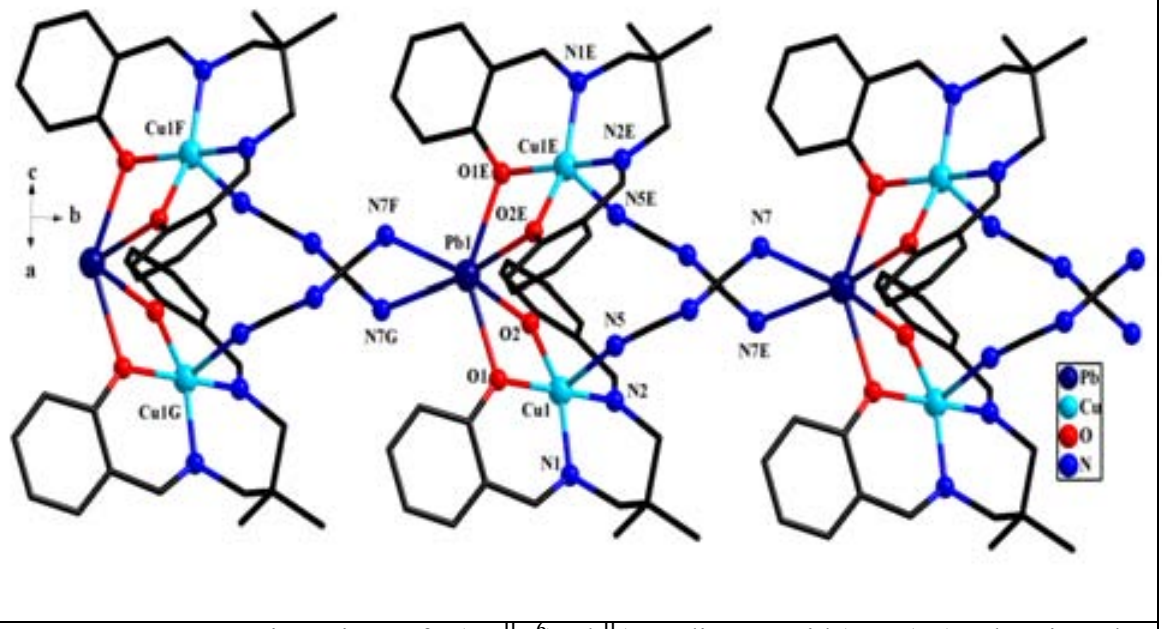

Figure 7.9. Perspective view of $[(Cu^{II}L^{6})_2Pb^{II}(\mu_{1,5}\text{-dicyanamide})_2]_n$ (**34**), showing the one-dimensional polymeric structure. All the hydrogen atoms are omitted for clarity. Symmetry: E, *–x*, *y*, 0.5*–z*; F, *–x*, *–*1*+y*, 0.5*–z*; G, *x*, *–*1*+y*, *z*.

The Pb^{II} center is hexacoordinated in **31** ($Pb^{II}O_6$), **33** ($Pb^{II}O_6$), **34** ($Pb^{II}O_4N_2$), and octacoordinated in **32** ($Pb^{II}O_8$). The coordination geometry of the Pb^{II} center in **34** is distorted octahedral with two phenoxo oxygen atoms (O1 and O1E) in the axial positions, while the coordination geometry of Pb^{II} center in **31**–**33**, cannot be defined by any regular geometry. The two copper(II) centers in the trinuclear units in **31** and **33** are crystallographically different, while those are symmetry related in **32** and **34**. Both the Cu^{II} centers in **31** and one Cu^{II} center (Cu1) in **33** are tetracoordinated and have distorted square planar geometry, while one Cu^{II} center (Cu2) in **33** and the symmetry related Cu^{II} centers in **32** and **34** are pentacoordinated and have distorted square pyramidal geometry; the axial position is occupied by a nitrile nitrogen atom (N5) of bridging dicyanamide for **34**, by a semicoordinated nitrate oxygen atom (O3; which also links Pb^{II}) in **32** and by a semicoordinated perchlorate oxygen atom (O7A) for the Cu2 center in **33**.

The selected bond lengths and angles and some other structural parameters of **31**–**34**, are compared in Table 7.2, while the bond distances and angles of the individual compounds are listed in Tables 7.3–7.6. The overall range of Cu^{II}–O(phenoxo) and Cu^{II}–

N(imine) bond distances in the four compounds are 1.890–1.981 and 1.934–2.010 Å. For a particular copper(II) center, Cu^{II}–N(imine) bond distances are slightly greater than Cu^{II}–O(phenoxo) bond distances. As usual, the bond distances involving the apical ligand in **32**, **33** and **34** are significantly longer, 2.715 (semicoordinated), 2.765 (semicoordinated) and 2.243 Å, respectively. The overall ranges of the *transoid* angles and *cisoid* angles in **31**–**34**, are 159.40–171.58° and 79.19–106.42°. As listed in Table 7.2, average deviation of the N and O atoms ($d_{N/O}$) and displacement of the copper(II) center(s) (d_{Cu}) from the corresponding least-squares $N(imine)_2O(phenoxo)_2$ plane and the discrimination parameter (τ) indicate distorted square planar / square pyramidal coordination geometry of copper(II).

Table 7.2. Comparative Structural Parameters (Distances in Å and Angles in deg) in the Coordination Environment of the Metal Centers in **31**–**34**.

	31	**32**	**33**	**34**
Cu–O(phenoxo)	1.922–1.955	1.931,1.952	1.890–1.940	1.950, 1.981
Cu–N(imine)	1.953–1.968	1.977,1.986	1.934–1.976	1.976, 2.010
Cu–apical ligand [a]	—	2.715	2.765	2.243
Cisoid angles	79.84–97.3	79.19–106.42	80.24–99.87	80.73–105.67
Transoid angles	166.0–169.95	169.78,170.95	162.2–171.58	159.40,167.94
τ	—	0.019	0.0483(for Cu2)	0.142
$d_{N/O}$ [b]	0.1141, 0.1820	0.0923	0.0425, 0.2680	0.0855
d_{Cu} [b]	(+)0.0153, (+)0.0012	(+)0.0146	(–)0.0015, (+)0.0290	(+)0.2519
δ_{arene} [c]	13.43, 44.17	10.91	3.42, 33.31	51.23
δ_{copper} [c]	13.87	2.65	23.81	64.60
Pb^{II}–O(phenoxo)	2.405–2.553	2.533, 2.604	2.444–2.703	2.390, 2.494
Pb^{II}–O[d](other ligand)	2.745, 2.766	2.721, 2.748	2.412, 2.564	—
Pb^{II}–N[d](other ligand)	—	—	—	2.890
O/N–Pb^{II}–O/N angles	59.42–160.31	46.23–156.83	52.1–164.08	—
Cisoid angles	—	—	—	62.79–110.26
Transoid angles	—	—	—	139.78–171.63
d_{Pb} [b]	—	—	—	0.000
d_{plane} [b]	—	—	—	0.166
Cu^{II}–Pb^{II}	3.4981, 3.5385	3.4543	3.4176, 3.4910	3.5244
Cu^{II}–O(phenoxo)–Pb^{II}	102.00–106.77	98.15, 99.95	95.45–104.13	104.28, 107.11

[a] Nitrate oxygen atom in **32**, perchlorate oxygen atom in **33**, dicyanamide nitrogen atom in **34**.

[b] d_{Cu} / d_{Pb} are the displacements of the Cu^{II} / Pb^{II} center, and $d_{N/O}$ /d_{plane} are the average deviations of the constituent atom from the corresponding least-squares plane.

[c] Dihedral angle between two arene rings/ dihedral angle between basal planes of two either crystallographically different or symmetry related Cu^{II} centers.

[d] Perchlorate oxygen atom in **31**, nitrate oxygen atom in **32**, carboxylate oxygen atom in **33**, dicyanamide nitrogen atom in **34**.

Table 7.3. Selected Bond Lengths (Å) and Angles (deg) of $[(Cu^{II}L^{8})_2Pb^{II}(ClO_4)_2]$ (**31**).

Bond lengths		**Bond Angles**			
Cu(II) center		Cu(II) center		Pb(II) center	
Cu1–O1	1.955(4)	N1–Cu1–O2	169.95(18)	O3–Pb1–O2	160.31(14)
Cu1–O2	1.922(4)	N2–Cu1–O1	168.3(2)	O4–Pb1–O9A	91.5(3)
Cu1–N2	1.968(5)	N1–Cu1–N2	96.8(2)	O1–Pb1–O5A	78.27(71)
Cu1–N1	1.967 (5)	N1–Cu1–O1	92.42(18)	O3–Pb1–O4	61.13(14)
Cu2–N3	1.953(6)	O1–Cu1–O2	79.84(15)	O4–Pb1–O1	74.16(13)
Cu2–N4	1.965(5)	N2–Cu1–O2	91. 7(2)	O1–Pb1–O2	59.42(12)
Cu2–O3	1.924(4)	N3–Cu2–O4	166.0(2)	O2–Pb1–O9A	76.3(2)
Cu2–O4	1.940(4)	N4–Cu2–O3	167.1(2)	O9A–Pb1–O5A	138.45(71)
		N3–Cu2–O3	90.6(2)	O3–Pb1–O5A	85.45(58)
Cu1···Pb1	3.5385(7)	N4–Cu2–N3	97.3(3)	O4–Pb1–O5A	129.25(70)
Cu2···Pb1	3.4981(7)	O4–Cu2–N4	92.7(2)	O1–Pb1–O3	103.06(13)
		O3–Cu2–O4	81.49(17)	O2–Pb1–O5A	98.46(59)
Pb(II) center				O9A–Pb1–O3	113.3(3)
Pb1–O1	2.465(4)	Cu1–O1–Pb1	105.80(16)	O2–Pb1–O4	102.78(13)
Pb1–O2	2.553(4)	Cu1–O2–Pb1	103.60(15)	O9A–Pb1–O1	127.7(2)
Pb1–O5A	2.766(34)	Cu2–O3–Pb1	102.00(16)		
Pb1–O9A	2.745(11)	Cu2–O4–Pb1	106.77(17)		
Pb1–O3	2.548(4)				
Pb1–O4	2.405(4)				

Table 7.4. Selected Bond Lengths (Å) and Angles (º) of $[(Cu^{II}L^{6})_2Pb^{II}(NO_3)_2]$ (**32**).

Bond lengths		**Bond Angles**			
Cu(II) center		Cu(II) center		Pb(II) center	
Cu1–N1	1.986(3)	O1–Cu1–N2	169.78(1)	O1–Pb1–O2	58.59(7)
Cu1–N2	1.977(3)	O2–Cu1–N1	170.95(11)	O5–Pb1–O3	46.23(8)
Cu1–O1	1.931(2)	O1–Cu1–O2	80.71(9)	O1–Pb1–O3	69.12(8)
Cu1–O2	1.952(2)	O1–Cu1–N1	91.75(10)	O2–Pb1–O5	117.11(7)
Cu1–O3	2.715(3)	O2–Cu1–N2	91.53(12)	O1–Pb1–O5	83.92(8)
		N1–Cu1–N2	96.52(12)	O2–Pb1–O3	72.55(8)
Pb1(II) center		O3–Cu1–N1	91.82(10)	O5–Pb1–O5C	126.12(12)
Pb1–O1	2.604(2)	O3–Cu1–N2	106.42(11)	O3–Pb1–O3C	156.83(12)
Pb1–O2	2.533(2)	O3–Cu1–O1	79.19(90)	O1–Pb1–O5C	82.62(7)
Pb1–O3	2.721(3)	O3–Cu1–O2	81.90(9)	O1C–Pb1–O3	117.41(8)
Pb1–O5	2.748(3)			O1–Pb1–O1C	150.01(10)
		Cu1–O1–Pb1	98.15(9)	O1–Pb1–O2C	150.52(7)
Cu1···Pb1	3.4543(4)	Cu1–O2–Pb1	99.95(9)	O2–Pb1–O5C	98.98(9)
				O2–Pb1–O3C	91.65(8)
				O2–Pb1–O2C	95.06(10)
				O3–Pb1–O5C	150.90(9)
				O3–Pb1–O2C	91.65(8)

Table 7.5. Selected Bond Lengths (Å) and Angles (deg) of $[\{(Cu^{II}L^{6})_2Pb^{II}\}_2(\mu\text{-adipate})](ClO_4)_2\cdot 2H_2O$ (**33**).

Bond lengths		**Bond Angles**			
Cu(II) center		Cu(II) center		Pb(II) center	
Cu1–O1	1.924(4)	N1–Cu1–O2	171.15(19)	O4–Pb1–O2	164.08(12)
Cu1–O2	1.940(4)	N2–Cu1–O1	171.58(17)	O3–Pb1–O5	84.72(17)
Cu1–N2	1.968(5)	N1–Cu1–N2	96.8(2)	O2–Pb1–O5	69.62(18)
Cu1–N1	1.976(5)	N1–Cu1–O1	91.35(18)	O3–Pb1–O2	133.80(12)
Cu2–N3	1.940(5)	O1–Cu1–O2	80.24(16)	O4–Pb1–O3	60.93(13)
Cu2–N4	1.934(5)	N2–Cu1–O2	91.75(18)	O4–Pb1–O5	110.9(2)
Cu2–O3	1.932(4)	N3–Cu2–O4	165.1(2)	O2–Pb1–O1	57.22(12)
Cu2–O4	1.890(4)	N4–Cu2–O3	162.2(2)	O1–Pb1–O5	82.4(2)
Cu2–O7A	2.765(15)	N3–Cu2–O3	92.53(19)	O3–Pb1–O1	82.47(13)
		N4–Cu2–N3	91.9(2)	O4–Pb1–O1	138.46(12)
Cu1···Pb1	3.4910(6)	O4–Cu2–N4	94.2(2)	O2–Pb1–O6	87.4(2)
Cu2···Pb1	3.4176(7)	O3–Cu2–O4	85.84(18)	O5–Pb1–O6	52.1(3)
		O7A–Cu2–O3	99.87(37)	O6–Pb1–O1	131.1(2)
Pb(II) center		O7A–Cu2–O4	81.29(33)	O6–Pb1–O3	106.7(2)
Pb1–O1	2.481(4)	O7A–Cu2–N3	84.41(33)	O6–Pb1–O4	81.3(2)
Pb1–O2	2.703(4)	O7A–Cu2–N4	97.76(35)		
Pb1–O5	2.412(6)				
Pb1–O6	2.564(7)	Cu1–O1–Pb1	104.13(15)		
Pb1–O3	2.444(4)	Cu1–O2–Pb1	96.14(15)		
Pb1–O4	2.674(4)	Cu2–O3–Pb1	102.04(17)		
		Cu2–O4–Pb1	95.45(16)		

Table 7.6. Selected Bond Lengths (Å) and Angles (deg) of $[(Cu^{II}L^{6})_2Pb^{II}(\mu_{1,5}$-dicyanamide$)_2]_n$ (**34**).

Bond lengths		**Bond Angles**			
Cu(II) center		Cu(II) center		Pb(II) center	
Cu1–O1	1.950(2)	N1–Cu1–O2	159.40(9)	O1–Pb1–O2	62.79(6)
Cu1–O2	1.981(2)	N2–Cu1–O1	167.94(10)	O1–Pb1–N7G	110.26(8)
Cu1–N1	2.010(2)	N1–Cu1–N2	94.37(9)	O2–Pb1–N7G	171.63(8)
Cu1–N2	1.976(2)	N1–Cu1–O1	91.05(8)	O1–Pb1–N7F	100.41(9)
Cu2–N5	2.243(3)	O1–Cu1–O2	80.73(8)	O2–Pb1–N7F	96.38(7)
		N2–Cu1–O2	90.56(9)	N7F–Pb1–N7G	79.95(9)
Cu1···Pb1	3.5244(5)	N5–Cu2–O1	99.66(10)	O1–Pb1–O2E	87.91(7)
		N5–Cu2–O2	105.67(9)	O1–Pb1–O1E	139.78(9)
Pb(II) center		N5–Cu2–N1	94.27(10)	O2–Pb1–O1E	87.91(7)
Pb1–O1	2.494(2)	N5–Cu2–N2	90.69(11)	O2–Pb1–O2E	88.22(9)
Pb1–O2	2.390(2)			O2E–Pb1–N7F	171.63(8)
Pb1–O1E	2.494(2)	Cu1–O1–Pb1	104.28(7)		
Pb1–O2E	2.390(2)	Cu1–O2–Pb1	107.11(8)		
Pb1–N7G	2.890(3)				
Pb1–N7F	2.890(3)				

As expected, the bond distances involving Pb^{II} are much longer than those of the bond distances involving Cu^{II} (excluding semicoordinated bonds involving Cu^{II}); the ranges of Pb^{II}–O/N bond distances in **31**, **32**, **33**, and **34** are 2.405–2.766, 2.533–2.748, 2.412–2.703 and 2.390–2.890 Å. The ranges of O–Pb–O/O–Pb–N/N–Pb–N bond angles in **31**–**34**, are 59.42–160.31, 46.23–156.83, 52.1–164.08 and 62.79–171.63° respectively. As already mentioned, only the geometry of Pb^{II} in **34** can be defined and that is highly distorted octahedral; the ranges of *cisoid* and *transoid* angles are 62.79–110.26° and 139.78–171.63°.

In trinuclear cores, as in **31**–**34**, two types of parameters may be considered as an indication of the relative planarity of the trinuclear moiety as a whole. These are the dihedral angle (δ_{arene}) between the two arene rings of a ligand and the dihedral angle (δ_{copper}) between the basal planes of the two copper(II) environments. If both δ_{arene} and δ_{copper} are smaller, we can say the trinuclear core is more planar and vice versa. As listed in Table 7.2: (i) Both δ_{arene} (51.23°) and δ_{copper} (64.60°) values are the largest for **34**; (ii) For **33**, although one δ_{arene} (3.42°) is the smallest in the series, the second δ_{arene} (33.31°) and the δ_{copper} (23.81°) are larger than the δ_{arene} (10.91°) and the δ_{copper} (2.65°) in **32**; (iii) Both δ_{arene} (13.43 and 44.17°) and δ_{copper} (13.87°) values in **31** are larger than those in **32** (δ_{arene} = 10.91 and δ_{copper} = 2.65°). All these indicate that the trinuclear core is the most distorted in **34** and the most planar in **32**, while the extent of planarity/distortion of **31**/**33** is in between those of **32** and **34**.

7.3.3. Lone Pair Functionality of Pb^{II} in 31–34

The lone pair of outer electrons of Pb^{II}, which is related to the so-called ‘inert pair effect’, may also distort the coordination geometry of the metal ion.[72–76] In general for any coordination number, the coordination geometry of Pb^{II} can be categorized as holodirected and hemidirected.[73–75] In the holodirected case, the bonds to ligand atoms are distributed throughout the surface of an encompassing globe.[73] In contrast, in the hemidirected case, the bonds to ligand atoms are directed towards only part of an encompassing globe, i.e., there is an identifiable void in the distribution of bonds to the

ligands.[73] The lead(II)–ligand bond distances involving the ligands near to the lone pair should also be greater than those involving ligands opposite to the lone pair. Therefore, if such a gap and such a specific difference in bond distances exist, it is considered as the evidence of a stereochemically active lone pair of electrons. Clearly, such a lone pair functionality is accompanied with hemidirected, i.e., significantly distorted, coordination geometry. However, only the difference in bond distances has also been considered as the existence of stereochemically active lone pair of electrons in some holodirected homoleptic systems.[73,75,76] It has been revealed from the analyses of the CSD structures that coordination number of lead(II) is a governing parameter for the lone pair to be stereochemically active or inactive[73]: (i) All systems with coordination number 2–5 have active lone pair (hemidirected geometry); (ii) All systems with coordination numbers 9 and 10 have inactive lone pair (holodirected geometry); (iii) For systems with coordination numbers 6–8, some have active (hemidirected geometry) while some others have inactive (holodirected geometry) lone pair. These indicate that directional effect of the lone pair of electrons is diminished with the crowding of the ligands.[73] It is also worth mentioning that the concerned lone pair functionality is a metal-centered property and therefore asymmetry in ligand environment (i.e., different types of ligands – electronically and sterically) should hinder the understanding of whether the lone pair of electron is steochemically active or not.

The coordination numbers of lead(II) in **31**, **33**, and **34** is 6, while that in **32** is 8. As the coordination numbers lie in the range 6–8, the possibility of the existence of an active lone pair is definitely reduced in **31**–**34**. Moreover, the ligand environment is highly asymmetric, which even includes chelating/bridging compartments and so it seems to be problematic to judge the effect of lone pair functionality. In spite of that, interestingly, the above mentioned type of gap and the above mentioned type of specific difference in bond distances are observed in **31**, **32**, and **33** (Figure 7.10). For **31** where Pb^{II} is six-coordinated (Figure 7.10), the Pb1–O5A (perchlorate) and Pb1–O9A (perchlorate) bond distances (2.766 and 2.745 Å respectively) are much longer than Pb1–O1 (phenoxo) and Pb1–O4 (phenoxo) bond distances (2.465 and 2.405 Å respectively) and O5A–Pb1–O9A angle is sufficiently obtuse, 138.45º, indicating that lone pair resides in between O5A and O9A (the region of gap). For **33** where Pb^{II} is six-coordinated

(Figure 7.10), the Pb1–O2 (phenoxo) and Pb1–O4 (phenoxo) bond distances (2.703 and 2.674 Å respectively) are much longer than Pb1–O3 (phenoxo) and Pb1–O5 (adipate) bond distances (2.444 and 2.412 Å respectively) and O2–Pb1–O4 angle is highly obtuse, 164.08º, indicating that lone pair resides in between O2 and O4 (the region of gap). For **32** where Pb^{II} is eight-coordinated (Figure 7.10), the Pb1–O5 (nitrate) and Pb1–O5C (nitrate) bond distances (2.748 Å) are significantly longer than Pb1–O2 (phenoxo) and Pb1–O2C (phenoxo) bond distances (2.533 Å) and O5–Pb1–O5C angle is sufficiently obtuse, 126.12º, indicating that lone pair resides in between O5 and O5C (the region of gap). So, in all these three cases, the lone pair of electron can be considered as stereochemically active and this effect is a crucial factor for the significant distortion of the coordination geometry of the metal ion. It is also interesting to note that, of the four phenoxo bond distances, those involving the location opposite to the lone pair are clearly the shortest and those involving the location near to the lone pair are clearly the longest: (i) For **31**, Pb1–O1 (2.465 Å) and Pb1–O4 (2.405 Å) are opposite to the lone pair and therefore shorter than the other two (Pb1–O2 = 2.553 and Pb1–O3 = 2.548 Å); (ii) For **33**, Pb1–O2 (2.703 Å) and Pb1–O4 (2.674 Å) are near to the lone pair and therefore significantly longer than Pb1–O3 (2.444 Å; it is in the region opposite to the lone pair) or Pb1–O1 (2.481 Å); (iii)) For **32**, Pb1–O2 and Pb1–O2C (2.533 Å) are opposite to the lone pair and therefore shorter than the other two (Pb1–O1/O1C = 2.604 Å).

In the case of **34**, although Pb1–N7F/N7G (dicyanamide) bond distances (2.890 Å) are much longer than Pb1–O2/O2E (phenoxo) bond distances (2.39 Å), the N7F–Pb1–N7G angle (79.95˚) is too small to consider this region as the required gap. Moreover, as already discussed, the coordination geometry of Pb^{II} here can be well defined as distorted octahedral. Therefore, it is evident that the lone pair in this compound is stereochemically inactive.

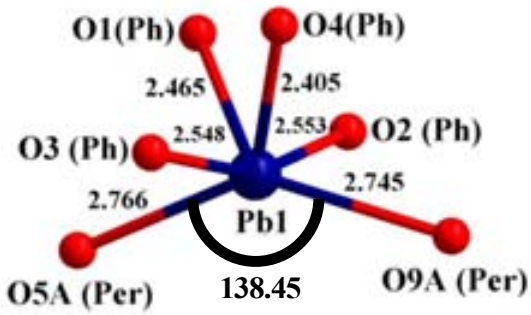

Complex 31

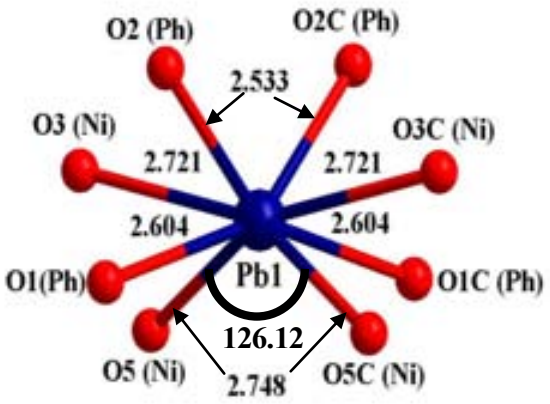

Complex 32

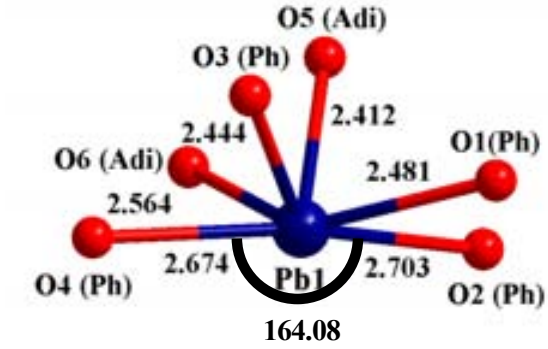

Complex 33

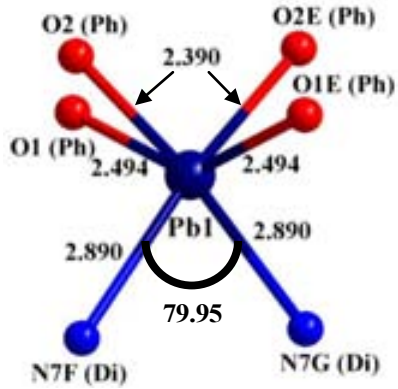

Complex 34

Figure. 7.10. Coordination environment of Pb^{II} centers in complexes **31**–**34**. Bond lengths are shown in Å. (Ph= phenoxo oxygen; Per= perchlorate oxygen; Ni= nitrate oxygen; Adi= adipate oxygen and Di= dicyanamide nitrogen atoms.

7.3.4. Comparison of the Compositions of 31–34 with Related Systems

A few copper(II)/nickel(II)/zinc(II)–lead(II) compounds have been previously reported from single-compartmental (salicylaldehyde/2-hydroxyacetophenone–diamine; H_2L^{single}) or double-compartmental (3-methoxy/ethoxysalicylaldehyde–diamine; H_2L^{double}) Schiff base ligands.[3,53–55,61–71] Those compounds are dinuclear $M^{II}Pb^{II}$,[53,54,61,66,67,69,70] trinuclear $M^{II}Pb^{II}M^{II}$ [63–65,67,68] or tetranuclear (dimer of dinuclear) $(M^{II}Pb^{II})_2$.[55,62,71] Clearly, in terms of types, the trinuclear ($Cu^{II}Pb^{II}Cu^{II}$) compounds **31** and **32** are similar to some previously reported systems. However, dimer of trinuclear

(hexanuclear) $(Cu^{II}Pb^{II}Cu^{II})_2$ compound **33** and trinuclear $(Cu^{II}Pb^{II}Cu^{II})$-based one-dimensional coordination polymer **34** are new types of systems containing copper(II) and lead(II).

7.3.5. Electrospray Ionization Mass Spectral Study

The electrospray ionization mass spectrum in positive mode (ESI-MS positive) of MeCN solution of **31**–**34** was recorded. The observed and simulated spectra of complexes are shown in Figures. 7.11─7.14 for compounds **31─34** respectively); the assigned species are listed in Table 7.7 (without drawing) and Tables 7.8.–7.11 (with drawing). The isotopic distributions of the observed and simulated peaks are matched well. A total of 16 types of species (**I**−**XVI**) are observed in the spectra of **31**−**34**. Two among the 16 species are mononuclear: (i) $[(Cu^{II}L^{8})+H^{+}]^{+}$ ($C_{17}H_{17}O_2N_2Cu$) (**I**; for **31**); (ii) $[(Cu^{II}L^{6})+H^{+}]^{+}$ ($C_{19}H_{21}O_2N_2Cu$) (**VII**; for **32**−**34**). Four among the 16 species are dinuclear: (i) $[Cu^{I}L^{8}Pb^{II}]^{+}$ ($C_{17}H_{16}O_2N_2CuPb$) (**III**; for **31**); (ii) $[Cu^{II}L^{8}Pb^{II}(ClO_4)]^{+}$ ($C_{17}H_{16}O_6N_2ClCuPb$) (**V**; for **31**); (iii) $[Cu^{II}L^{6}Na^{I}]^{+}$ ($C_{19}H_{20}O_2N_2CuNa$) (**VIII**; for **32**−**34**) and (iv) $[Cu^{II}L^{6}Pb^{II}(\text{dicyanamide})]^{+}$ ($C_{21}H_{20}O_2N_5CuPb$) (**XIV**; for **34**). Eight among the 16 species are trinuclear: (i) $[(Cu^{II}L^{8})_2Pb^{II}]^{2+}$ ($C_{34}H_{32}O_4N_4Cu_2Pb$) (**II**; for **31**); (ii) $[(Cu^{II}L^{8})_2Pb^{II}(ClO_4)]^{+}$ ($C_{34}H_{32}O_8N_4ClCu_2Pb$) (**VI**; for **31**); (iii) $[(Cu^{II}L^{6})_2+Na^{+}]^{+}$ ($C_{38}H_{40}O_4N_4Cu_2Na$) (**IX**; for **32**−**34**); (iv) $[(Cu^{II}L^{6})Na^{I}(Pb^{II}L^{A})]^{2+}$ (HL^{A} = Half condensed ligand corresponding to H_2L^{6}) ($C_{31}H_{37}O_3N_4CuPbNa$) (**X**; for **33**); (v) $[(Cu^{II}L^{6})_2Pb^{II}]^{2+}$ ($C_{38}H_{40}O_4N_4Cu_2Pb$) (**XI**; for **33** and **34**); (vi) $[\{Cu^{II}(MeCN)L^{6}\}_2Pb^{II}(L^{B})+H^{+}]^{2+}$ ($C_{49}H_{52}O_6N_6Cu_2Pb$) (HL^{B} = salicyaldehyde) (**XII**; for **33**); (vii) $[\{Cu^{II}(MeCN)L^{6}\}_2Na^{I}]^{+}$ ($C_{42}H_{46}O_4N_6Cu_2Na$) (**XV**; for **34**); (viii) $[(Cu^{II}L^{6})_2Pb^{II}(\text{dicyanamide})]^{+}$($C_{40}H_{40}O_4N_7Cu_2Pb$) (**XVI**; for **34**). Two among the 16 peaks are tetranuclear: (i) $[Pb^{II}(Cu^{II}L^{8})_3]^{2+}$ ($C_{51}H_{48}O_6N_6Cu_3Pb$) (**IV**; for **31**); (ii) $[Pb^{II}(Cu^{II}L^{6})_3]^{2+}$ ($C_{57}H_{60}O_6N_6Cu_3Pb$) (**XIII**; for **33** and **34**). To summarize, the ionic species in ESI-MS positive in terms of nuclearity are as follows: (i) Mononuclear Cu^{II} species: **31**–**34**; (ii) Dinuclear $Cu^{II}Pb^{II}$ species: **31**, **34**; (iii) Dinuclear $Cu^{I}Pb^{II}$ species: **31**; (iii) Dinuclear $Cu^{II}Na^{I}$ species: **32**–**34**; (iv) Trinuclear $Cu^{II}Pb^{II}Cu^{II}$ species: **31**, **33**, and **34**; (v) Trinuclear $Cu^{II}Na^{I}Cu^{II}$ species: **32**–**34**; (vi) Trinuclear $Cu^{II}Na^{I}Pb^{II}$ species: **33**; (vii) Tetranuclear star $Pb^{II}Cu^{II}_3$ species (Chart 7.2): **31**, **33**, and **34**.

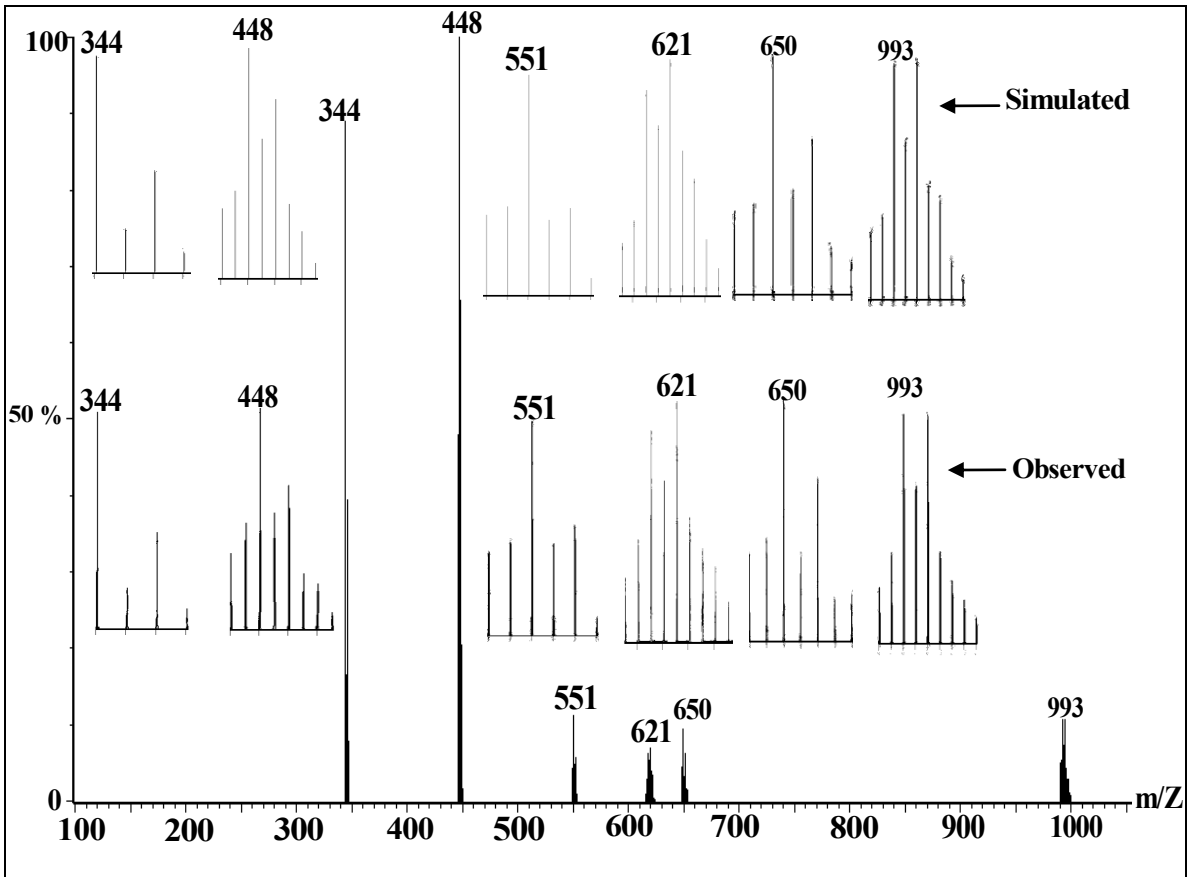

Figure 7.11. Electrospray ionization mass spectrum (ESI-MS positive) of $[(Cu^{II}L^{8})_2Pb^{II}(ClO_4)_2]$ (**31**) in MeCN showing observed and simulated isotopic distribution patterns.

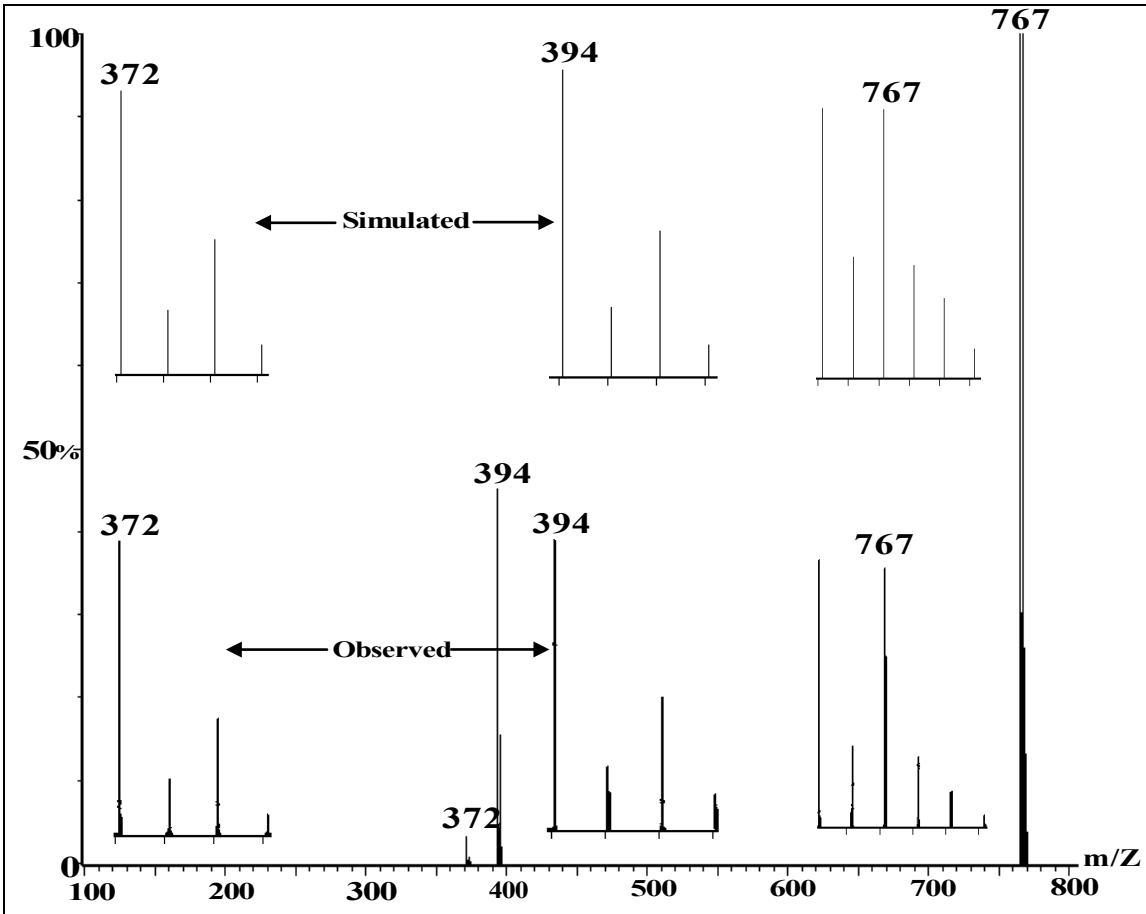

Figure 7.12. Electrospray ionization mass spectrum (ESI-MS positive) of $[(Cu^{II}L^{6})_2Pb^{II}(NO_3)_2]$ (**32**) in MeCN showing observed and simulated isotopic distribution patterns.

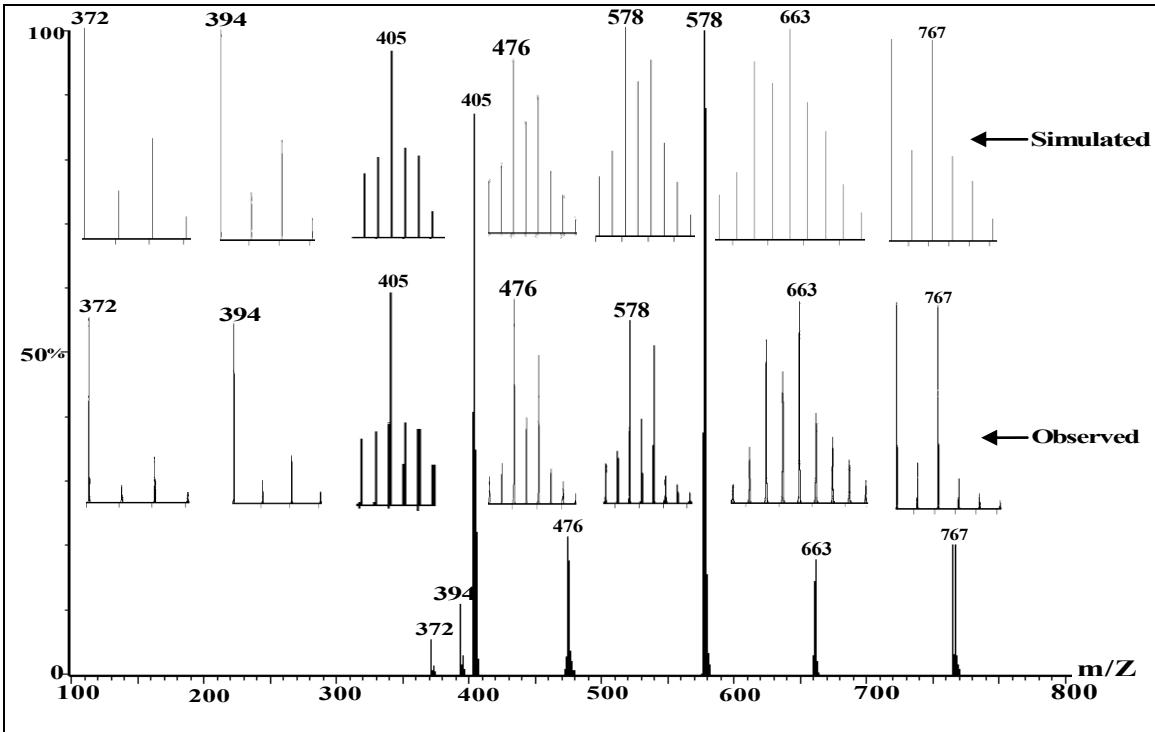

Figure 7.13. Electrospray ionization mass spectrum (ESI-MS positive) of $[\{(Cu^{II}L^{6})_2Pb^{II}\}_2(\mu\text{-adipate})](ClO_4)_2\cdot 2H_2O$ (**33**) in MeCN showing observed and simulated isotopic distribution patterns.

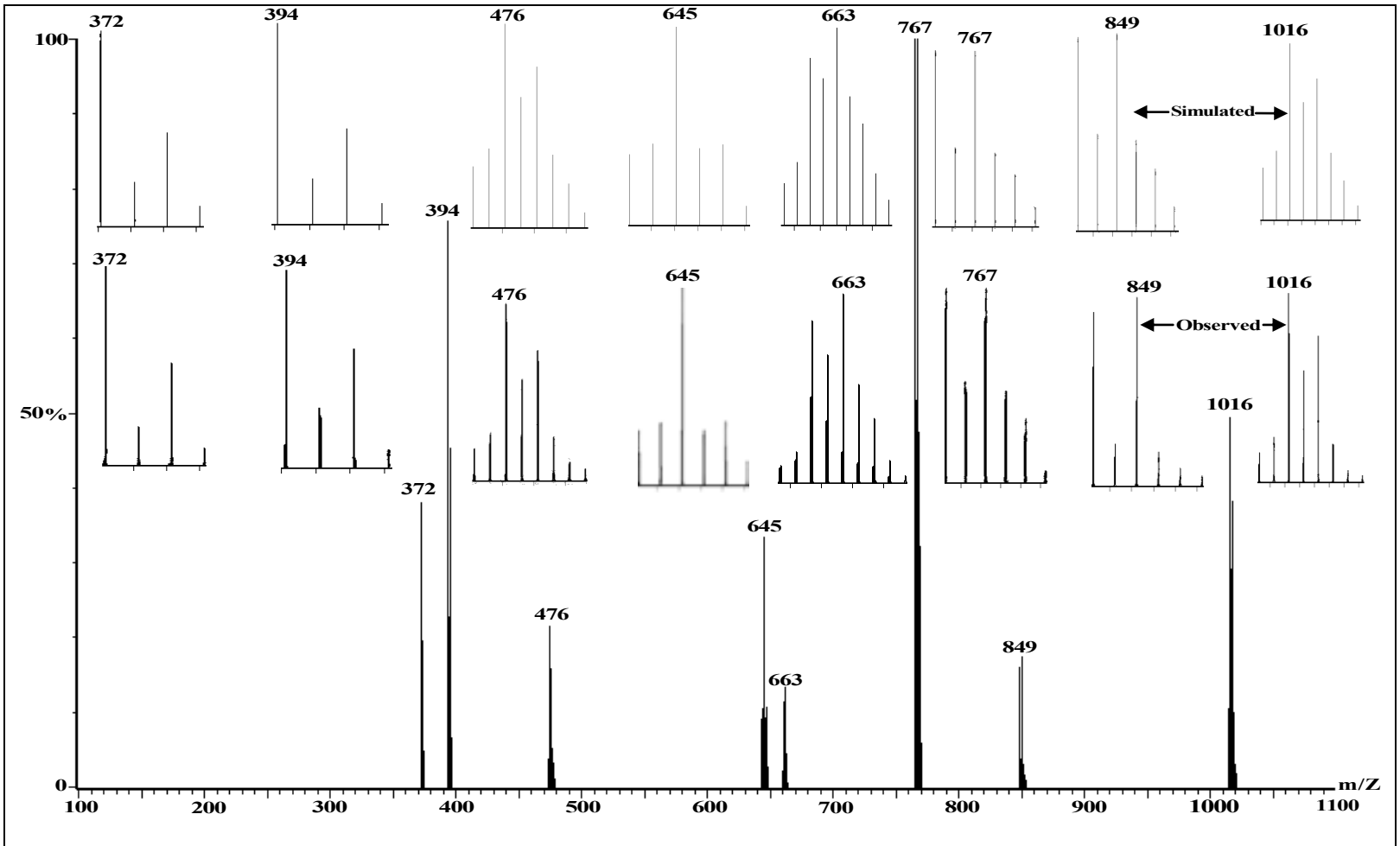

Figure 7.14. Electrospray ionization mass spectrum (ESI-MS positive) of $[(Cu^{II}L^{6})_2Pb^{II}(\mu_{1,5}\text{-dicyanamide})_2]_n$ (**34**) in MeCN showing observed and simulated isotopic distribution patterns.

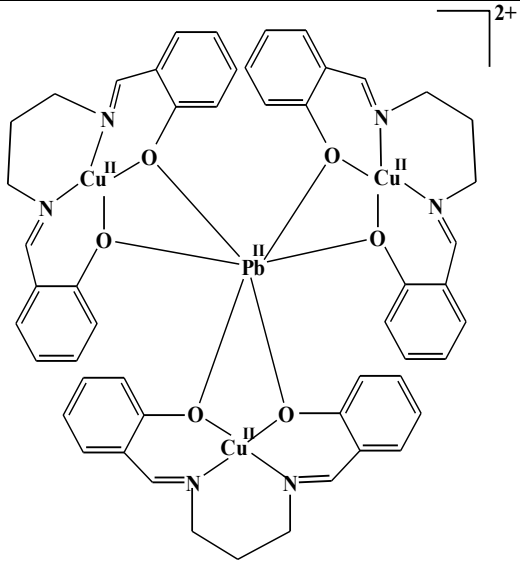

Chart 7.2. Star $Pb^{II}Cu^{II}_3$ Species in the ESI-MS of $[(Cu^{II}L^{8})_2Pb^{II}(ClO_4)_2]$ (**31**).

‘

Table 7.7. Composition, Formula, Formula Weight, m/z and Intensity of the Positive Ions Identified in ESI-MS (positive) of **31**–**34** [a].

Species Type	Composition of species	31	32	33	34
I	$[(Cu^{II}L^{8})+H^{+}]^{+}$ ($C_{17}H_{17}O_2N_2Cu$)	m/z = 344, Intensity = 95% Δ_l=1	—	—	—
II	$[(Cu^{II}L^{8})_2Pb^{II}]^{2+}$ ($C_{34}H_{32}O_4N_4Cu_2Pb$)	m/z = 448, Intensity = 100% Δ_l=0.5	—	—	—
III	$[Cu^{I}L^{8}Pb^{II}]^{+}$ ($C_{17}H_{16}O_2N_2CuPb$)	m/z = 551, Intensity = 12% Δ_l=1	—	—	—
IV	$[Pb^{II}(Cu^{II}L^{8})_3]^{2+}$ ($C_{51}H_{48}O_6N_6Cu_3Pb$)	m/z =621, Intensity = 8% Δ_l=0.5	—	—	—
V	$[Cu^{II}L^{8}Pb^{II}(ClO_4)]^{+}$ ($C_{17}H_{16}O_6N_2ClCuPb$)	m/z =650, Intensity = 10% Δ_l=1	—	—	—
VI	$[(Cu^{II}L^{8})_2 Pb^{II}(ClO_4)]^{+}$ ($C_{34}H_{32}O_8N_4ClCuPb$)	m/z =993 ,Intensity = 12% Δ_l=1	—	—	—
VII	$[(Cu^{II}L^{6})+H^{+}]^{+}$ ($C_{19}H_{21}O_2N_2Cu$)	—	m/z = 372, Intensity = 3% Δ_l=1	m/z = 372, Intensity = 3% Δ_l=1	m/z = 372, Intensity = 35% Δ_l=1
VIII	$[Cu^{II}L^{6}Na^{I}]^{+}$ ($C_{19}H_{20}O_2N_2CuNa$)	—	m/z = 394, Intensity = 50% Δ_l=1	m/z = 394, Intensity = 8% Δ_l=1	m/z = 394, Intensity = 80% Δ_l=1
IX	$[(Cu^{II}L^{6})_2Na^{I}]^{+}$ ($C_{38}H_{40}O_4N_4Cu_2Na$)	—	m/z = 767, Intensity = 100%, Δ_l=1	m/z = 767, Intensity = 20% Δ_l=1	m/z = 767, Intensity = 100%, Δ_l=1
X	$[(Cu^{II}L^{6})Na^{I}(Pb^{II}L^{A})]^{2+}$ (HL^{A} = Half condensed ligand corresponding to H_2L^{6}) ($C_{31}H_{37}O_3N_4Cu_1PbNa$)	—	—	m/z = 405, Intensity = 90%, Δ_l=0.5	—
XI	$[(Cu^{II}L^{6})_2Pb^{II}]^{2+}$ ($C_{38}H_{40}O_4N_4Cu_2Pb$)	—	—	m/z = 476, Intensity = 22% Δ_l=0.5	m/z = 476, Intensity = 22% Δ_l=0.5
XII	$[\{Cu^{II}(MeCN)L^{6}\}_2Pb^{II}(L^{B})+H^{+}]^{2+}$ (HL^{B} = salicyaldehyde) ($C_{49}H_{52}O_6N_6Cu_2Pb$)	—	—	m/z = 578, Intensity = 100%, Δ_l=0.5	—
XIII	$[Pb^{II}(Cu^{II}L^{6})_3]^{2+}$ ($C_{57}H_{60}O_6N_6Cu_3Pb$)	—	—	m/z = 663, Intensity = 20% Δ_l=0.5	m/z = 663, Intensity = 15% Δ_l=0.5
XIV	$[Cu^{II}L^{6}Pb^{II}(dicyanamide)]^{+}$ ($C_{21}H_{20}O_2N_5CuPb$)	—	—	—	m/z = 645, Intensity = 32% Δ_l=1
XV	$[\{Cu^{II}(MeCN)L^{6}\}_2Na^{I}]^{+}$ ($C_{42}H_{46}O_4N_6Cu_2Na$)	—	—	—	m/z = 849, Intensity = 20% Δ_l=1
XVI	$[(Cu^{II}L^{6})_2 Pb^{II}(dicyanamide)]^{+}$ ($C_{40}H_{40}O_4N_7Cu_2Pb$)	—	—	—	m/z = 1016, Intensity = 55%, Δ_l=1

[a] m/z values quoted in this table are for the major peak in the isotope pattern.

Table 7.8. The Composition, Empirical Formula, Peak Position and Relative Peak Intensity of the Species in the ESI-MS Positive Spectra of **31** in MeCN.

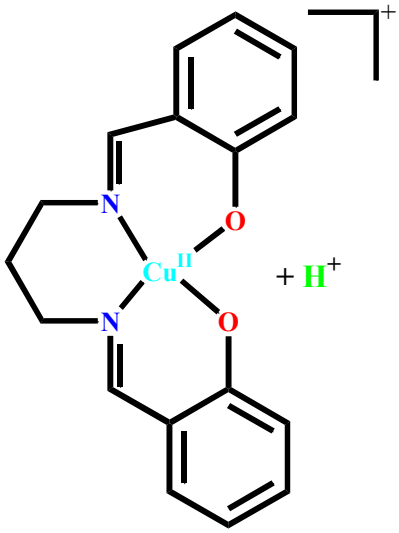	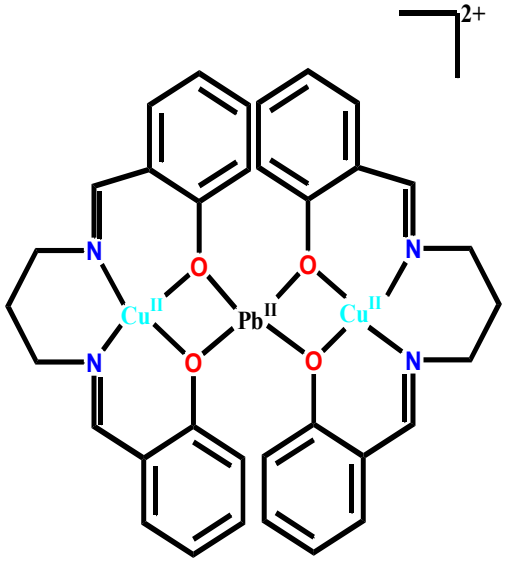
$[(Cu^{II}L^{8})+H^{+}]^{+}$ (**I**; $C_{17}H_{17}O_2N_2Cu$) m/z = 344, Intensity = 95%, Δ_l=1	$[(Cu^{II}L^{8})_2Pb^{II}]^{2+}$ (**II**; $C_{34}H_{32}O_4N_4Cu_2Pb$) m/z = 448, Intensity = 100%, Δ_l=0.5
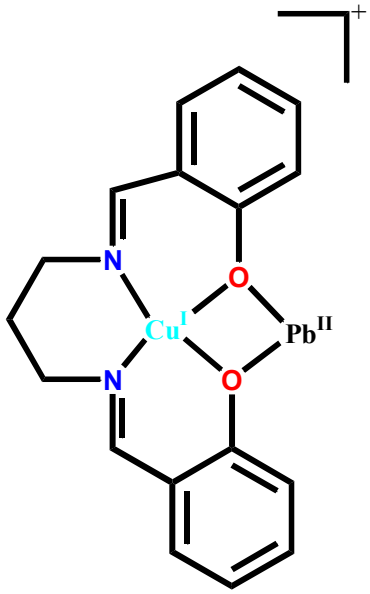	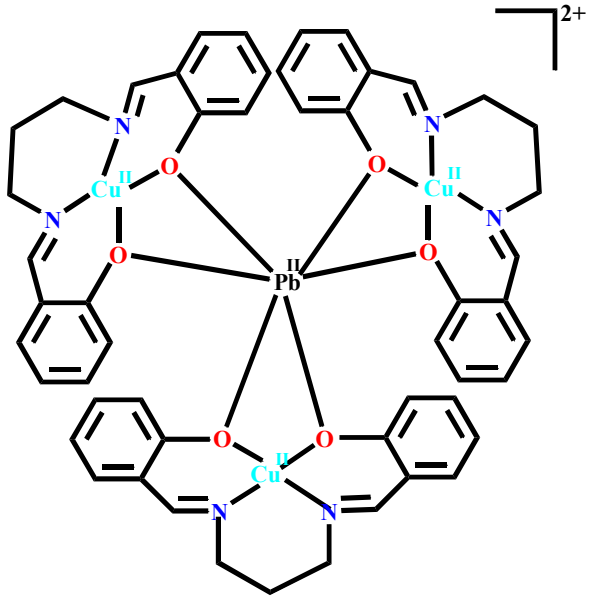
$[Cu^{I}L^{8}Pb^{II}]^{+}$ (**III**; $C_{17}H_{16}O_2N_2CuPb$) m/z = 551, Intensity = 12%, Δ_l=1	$[(Cu^{II}L^{8})_3Pb^{II}]^{2+}$ (**IV**; $C_{51}H_{48}O_6N_6Cu_3Pb$) m/z = 621, Intensity = 8% , Δ_l=0.5

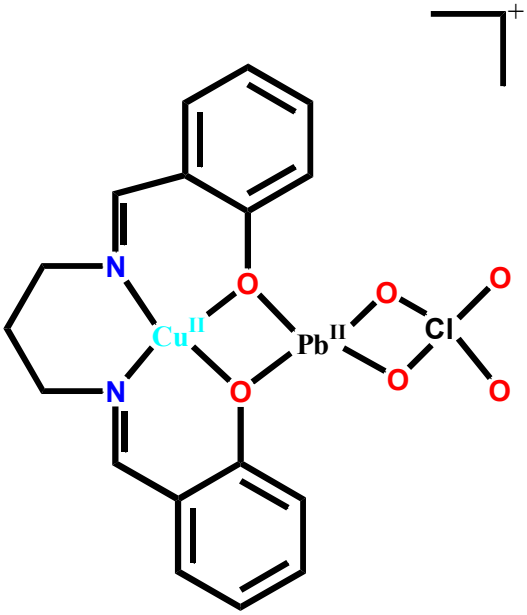	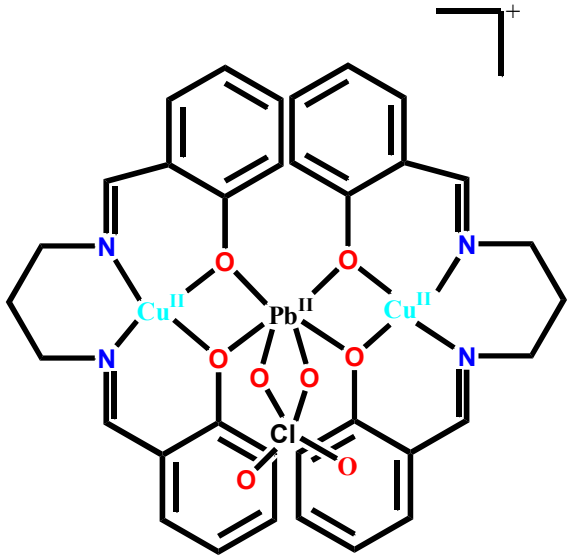
$[Cu^{II}L^{8}Pb^{II}(ClO_4)]^{+}$ (**V**; $C_{17}H_{16}O_6N_2ClCuPb$) m/z = 650, Intensity = 10%, Δ_l=1	$[(Cu^{II}L^{8})_2Pb^{II}(ClO_4)]^{+}$(**VI**;$C_{34}H_{32}O_8N_4ClCu_2Pb$) m/z = 993, Intensity = 12%, Δ_l=1

Table 7.9. The Composition, Empirical Formula, Peak Position and Relative Peak Intensity of the Species in the ESI-MS Positive Spectra of **32** in MeCN.

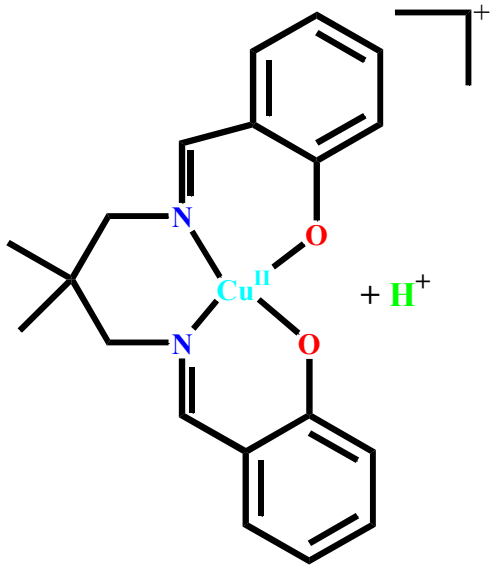	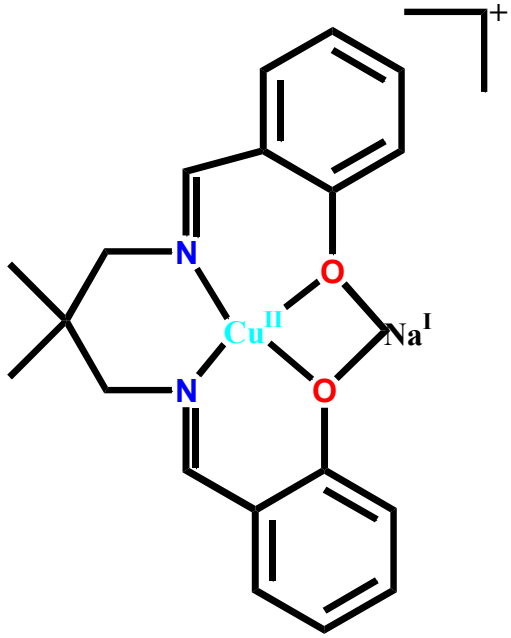
$[(Cu^{II}L^{6})+H^{+}]^{+}$ (**VII**; $C_{19}H_{21}O_2N_2Cu$) m/z = 372, Intensity = 3%, Δ_I=1	$[Cu^{II}L^{6}Na^{I}]^{+}$ (**VIII**; $C_{19}H_{20}O_2N_2CuNa$) m/z = 394, Intensity = 50%, Δ_I=1
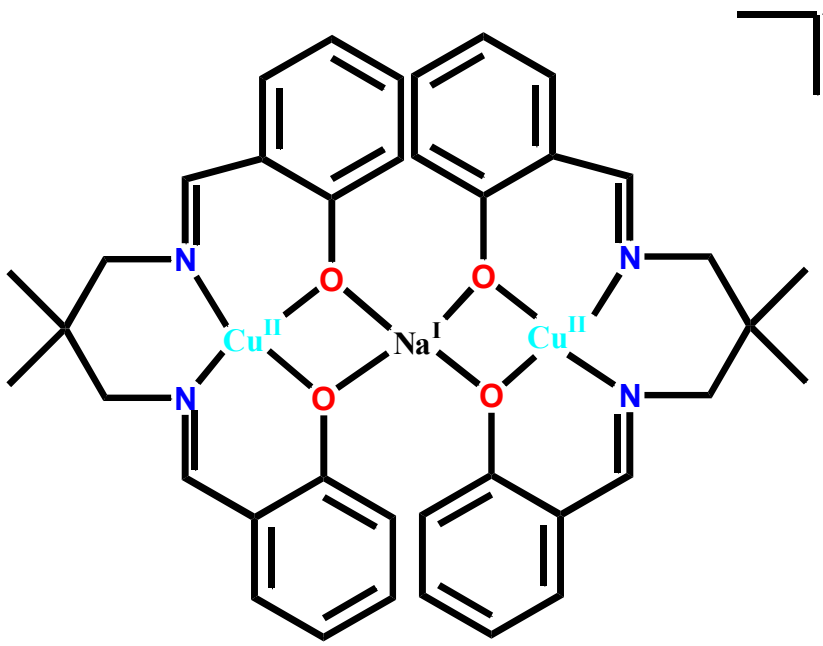	
$[(Cu^{II}L^{6})_2Na^{I}]^{+}$ (**IX**; $C_{38}H_{40}O_4N_4Cu_2Na$) m/z = 767, Intensity = 100%, Δ_I=1	

Table 7.10. The Composition, Empirical Formula, Peak Position and Relative Peak Intensity of the Species in the ESI-MS Positive Spectra of **33** in MeCN.

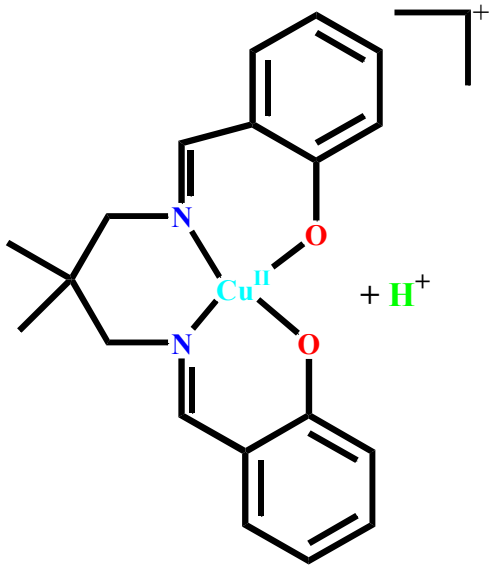	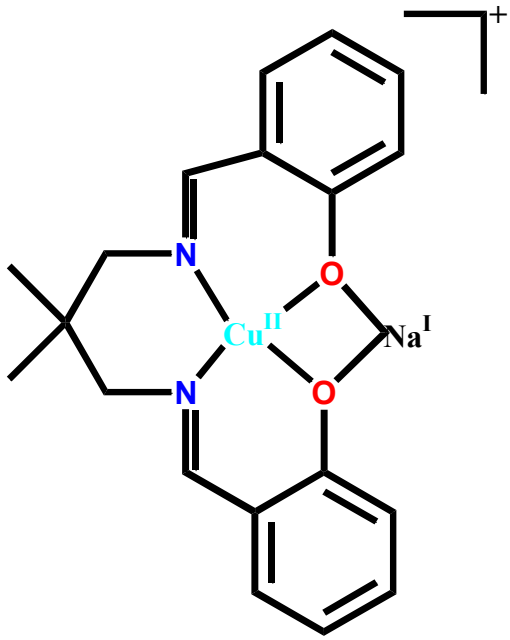
$[(Cu^{II}L^{6})+H^{+}]^{+}$ (**VII**; $C_{19}H_{21}O_2N_2Cu$) m/z = 372,I ntensity = 3% , Δ_I=1	$[Cu^{II}L^{6}Na^{I}]^{+}$ (**VIII**; $C_{19}H_{20}O_2N_2CuNa$) m/z = 394, Intensity = 8%, Δ_I=1
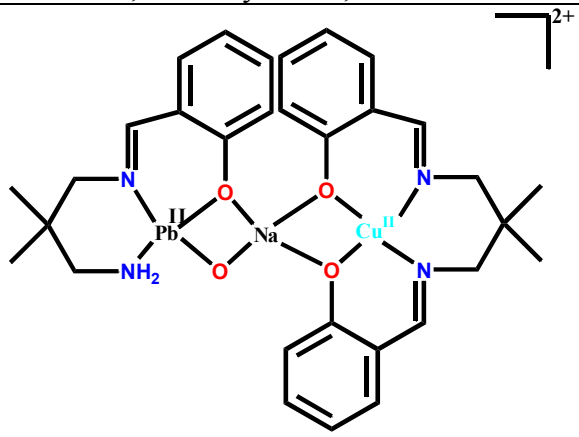	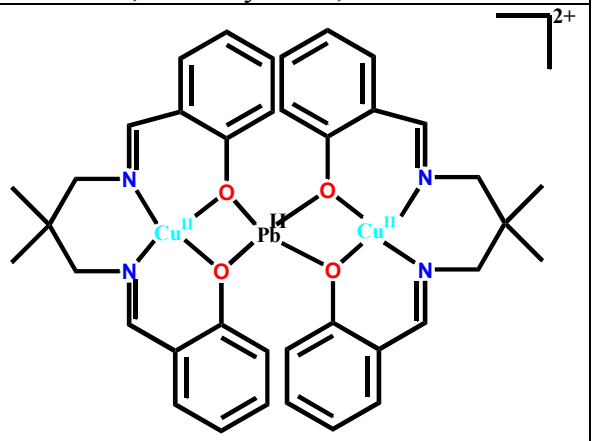
$[(Cu^{II}L^{6})Na^{I}(Pb^{II}L^{A})]^{2+}$ (HL^{A} = Half condensed ligand corresponding to H_2L^{6}) (**X**; $C_{31}H_{37}O_3N_4CuPbNa$) m/z = 405, Intensity = 90%, Δ_I=0.5	$[(Cu^{II}L^{6})_2Pb^{II}]^{2+}$ (**XI**; $C_{38}H_{40}O_4N_4Cu_2Pb$) m/z = 476, Intensity = 22%, Δ_I=0.5

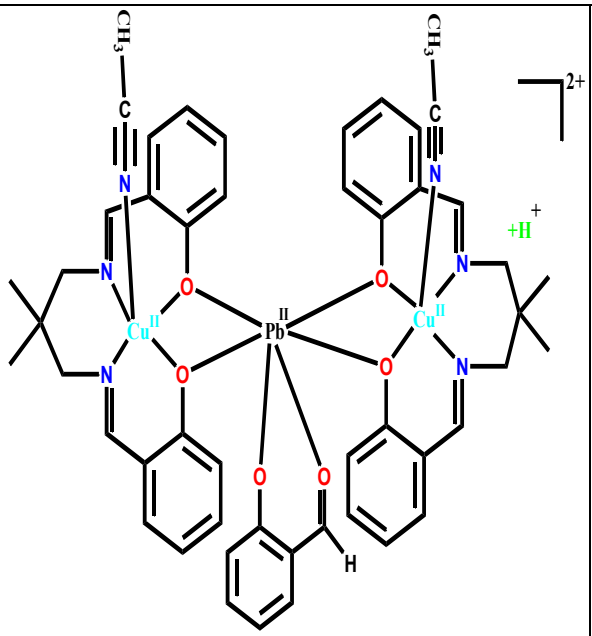

$[\{Cu^{II}(MeCN)L^{6}\}_{2}Pb^{II}(L^{B})+H^{+}]^{2+}$ (HL^{B} = salicyaldehyde) (**XII**; $C_{49}H_{52}O_{6}N_{6}Cu_{2}Pb$)
m/z = 578, Intensity = 100% , Δ_{I}=0.5

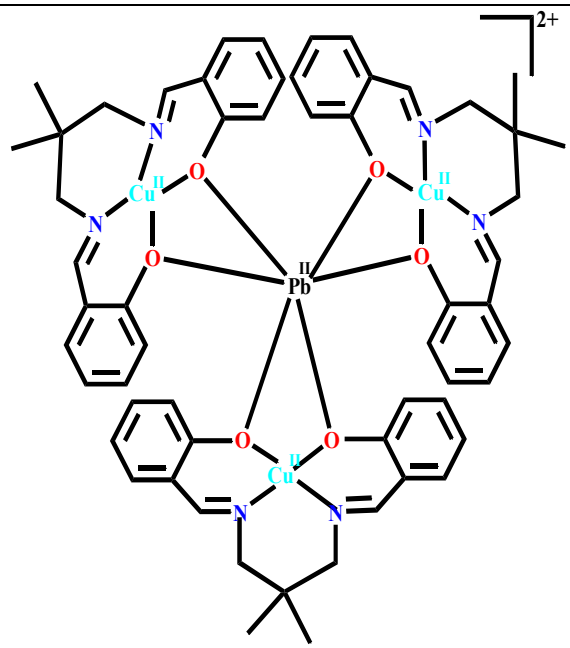

$[(Cu^{II}L^{6})_{3}Pb^{II}]^{2+}$ (**XIII**; $C_{57}H_{60}O_{6}N_{6}Cu_{3}Pb$)
m/z = 663, Intensity = 20% , Δ_{I}=0.5

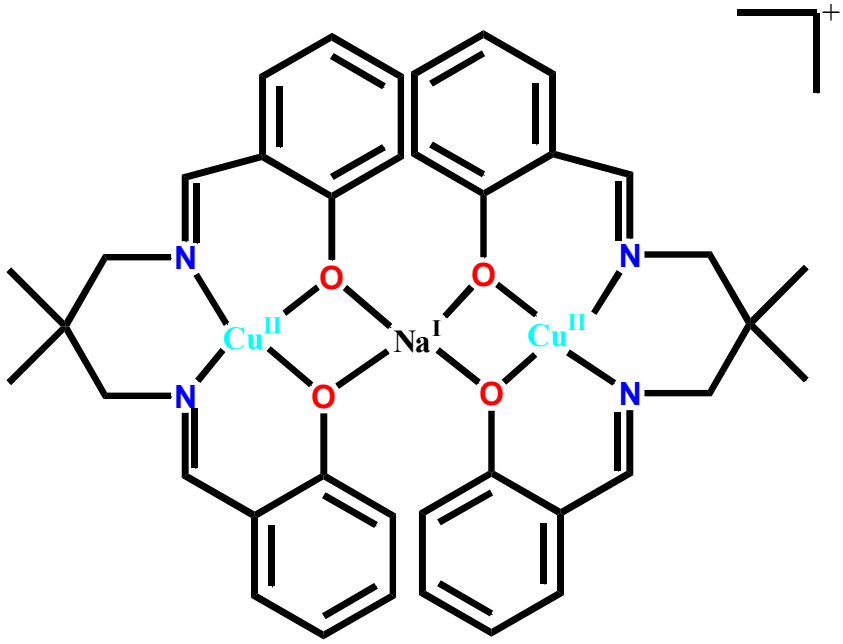

$[(Cu^{II}L^{6})_{2}Na^{I}]^{+}$ (**IX**; $C_{38}H_{40}O_{4}N_{4}Cu_{2}Na$)
m/z = 767, Intensity = 20% , Δ_{I}=1

Table 7.11. The Composition, Empirical Formula, Peak Position and Relative Peak Intensity of the Species in the ESI-MS Positive Spectra o f **34** in MeCN.

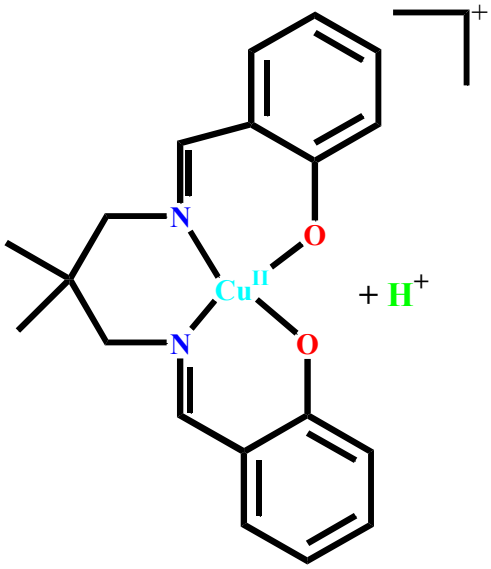	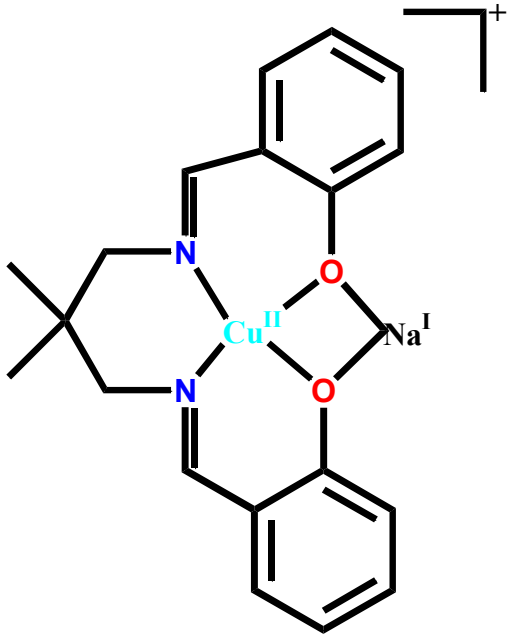
$[(Cu^{II}L^{6})+H^{+}]^{+}$ (**VII**; $C_{19}H_{21}O_2N_2Cu$) m/z = 372, Intensity = 35% , Δ_I=1	$[Cu^{II}L^{6}Na^{I}]^{+}$ (**VIII**; $C_{19}H_{20}O_2N_2CuNa$) m/z = 394, Intensity = 80%, Δ_I=1
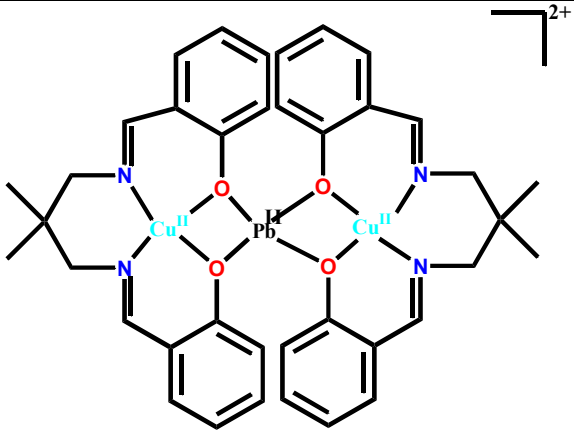	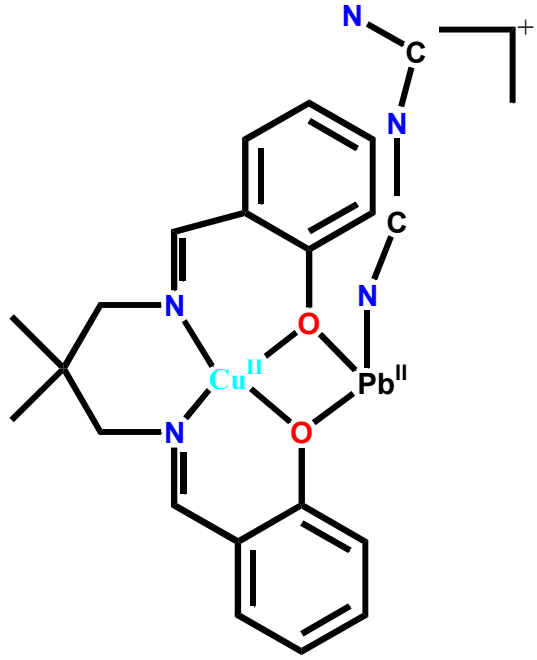
$[(Cu^{II}L^{6})_2Pb^{II}]^{2+}$ (**XI**; $C_{38}H_{40}O_4N_4Cu_2Pb$) m/z = 476, Intensity = 22%, Δ_I=0.5	$[Cu^{II}L^{6}Pb^{II}(dicyanamide)]^{+}$ (X**IV**; $C_{21}H_{20}O_2N_5CuPb$) m/z = 645, Intensity = 32%, Δ_I=1

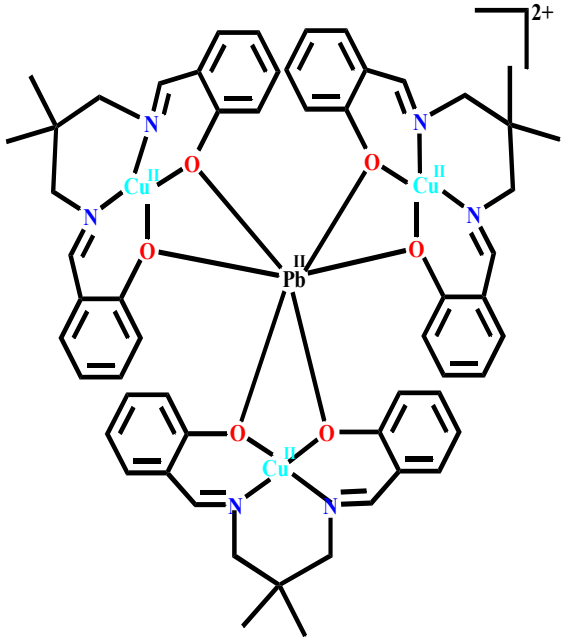	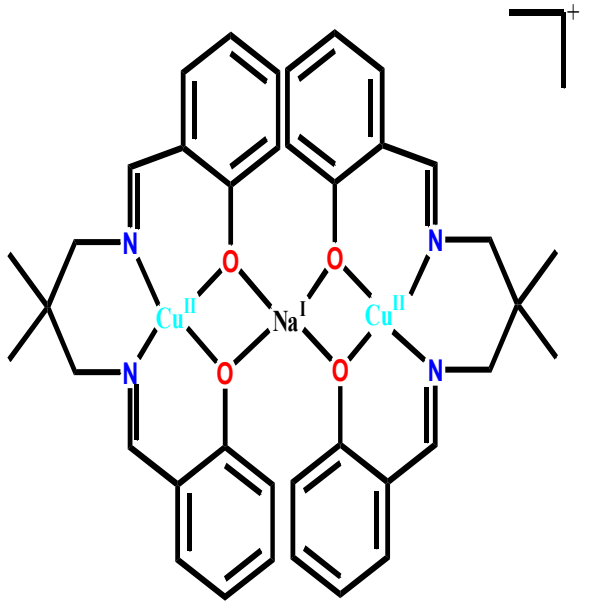
$[(Cu^{II}L^{6})_3Pb^{II}]^{2+}$ (**XIII**; $C_{57}H_{60}O_6N_6Cu_3Pb$) m/z = 663, Intensity = 15% , Δ_I=0.5	$[(Cu^{II}L^{6})_2Na^{I}]^{+}$ (**IX**; $C_{38}H_{40}O_4N_4Cu_2Na$) m/z = 767, Intensity = 100% , Δ_I=1
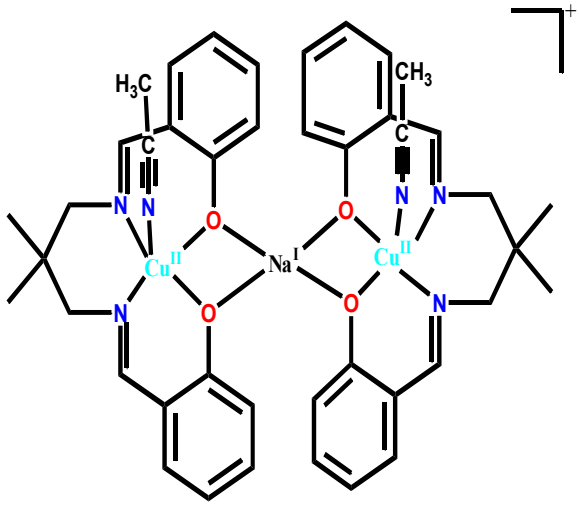	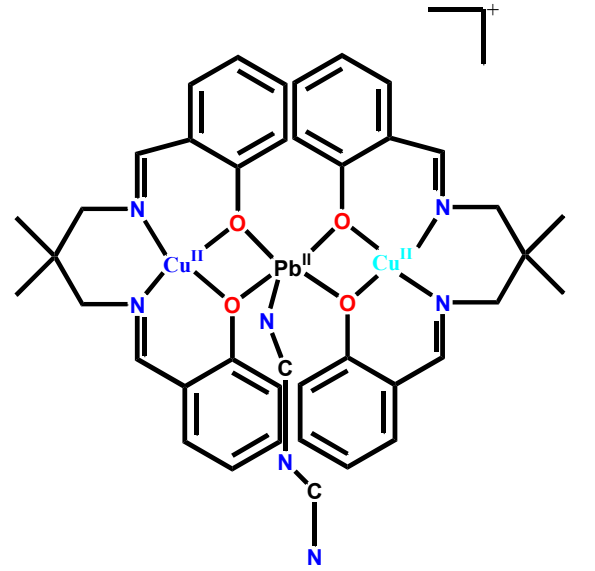
$[\{Cu^{II}(MeCN)L^{6}\}_2Na^{I}]^{+}$ (**XV**; $C_{42}H_{46}O_4N_6Cu_2Na$) m/z = 849, Intensity = 20%, Δ_I=1	$[(Cu^{II}L^{6})_2Pb^{II}(dicyanamide)]^{+}$ (**XVI**; $C_{40}H_{40}O_4N_7Cu_2Pb$) m/z = 1016, Intensity = 55%, Δ_I=1

7.3.6. Interesting Aspect in the ESI-MS Study

As already mentioned, the nature of the solid state composition of the heterometallic complexes derived from single-/double-compartmental Schiff base ligands depend on the particular ligand and metal–metal combination. For example: (i) 3-ethoxysalicylaldehyde–diamine ligands are known to stabilize cocrystals and the nature of cocrystals depend on metal–metal combinations;[47,50–61] (ii) *N*,*N*'-bis(salicylidene)-1,4-butanediamine ligand can stabilize a series of tetranuclear $M^{II}Cu^{II}_3$ stars (M = Cd, Zn, Cu, Ni, Mn).[27,35] In contrast, among a large number of previously published compounds including the four compounds in this investigation derived from H_2L^8/H_2L^6, not a single one is a star system.[3] However, the ESI-MS positive spectra of the trinuclear compound $[(Cu^{II}L^8)_2Pb^{II}(ClO_4)_2]$ (**31**) and dimer of trinuclear compound $[\{(Cu^{II}L^6)_2Pb^{II}\}_2(\mu\text{-adipate})](ClO_4)_2{\cdot}2H_2O$ (**33**) and trinuclear $Cu^{II}Pb^{II}Cu^{II}$–based one-dimensional (1D) compound $[(Cu^{II}L^6)_2Pb^{II}(\mu_{1,5}\text{-dicyanamide})_2]_n$ (**34**) indicate, interestingly, clear signature of the existence of $Pb^{II}Cu^{II}_3$ star systems $[Pb^{II}(Cu^{II}L^8)_3]^{2+}$ and $[Pb^{II}(Cu^{II}L^6)_3]^{2+}$.

7.4. Conclusions

The four compounds being reported herein are trinuclear, $[(Cu^{II}L^8)_2Pb^{II}(ClO_4)_2]$ (**31**) and $[(Cu^{II}L^6)_2Pb^{II}(NO_3)_2]$ (**32**), or dimer of trinuclear, $[\{(Cu^{II}L^6)_2Pb^{II}\}_2(\mu\text{-adipate})](ClO_4)_2{\cdot}2H_2O$ (**33**), or one-dimensional coordination polymer, $[(Cu^{II}L^6)_2Pb^{II}(\mu_{1,5}\text{-dicyanamide})_2]_n$ (**34**). This report presents first utilization of the incorporation of secondary organic/inorganic bridging ligands as the spacers to assemble the heterometallic copper(II)–lead(II) nodes from Schiff base ligands, leading to the stabilization of dimer of trinuclear compound **3** and trinuclear $Cu^{II}Pb^{II}Cu^{II}$–based one-dimensional (1D) compound **34**.

ESI-MS positive reveals the stabilization of ionic species (having charges 1+ and 2+) of various nuclearity, mono/di/tri/tetranuclear; the tetranuclear species are metal (Pb^{II}) centered $Pb^{II}Cu^{II}_3$ stars and such species are observed in the ESI-MS positive of three (**31**, **33** and **34**) of the four compounds. While mono/di/trinuclear species are common species in solid state also, the tetranuclear star species in solid state are unusual and dependent on the particular Schiff base ligand.[27,35] Notably, there is neither any

report of the stabilization of star species in the H_2L^8/H_2L^6 ligand environment nor any report of a star compound with Pb^{II} as the central metal ion from any type of ligands.[3] From those perspectives, the observation of the star $Pb^{II}Cu^{II}_3$ species (although in gaseous state) in the ESI-MS positive of three compounds in this investigation may be considered as interesting. Clearly, ESI-MS studies of the heterometallic systems may be undertaken in future studies for the new compounds as well as for the known related heterometallic compounds with the expectation to get the signature of some unusual species.

It is known that stereochemically active lone pair of electrons of lead(II) may or may not exist if coordination number is in the range 6–8; in fact, there is a report that the total no of Pb^{II} compounds having coordination number 6–8 and also having active lone pair is less than the total no of Pb^{II} compounds having coordination no. 6–8 and also having inactive lone pair.[73] It is also worth mentioning that in heteroleptic Pb^{II} compounds, it is complicated to identify whether the lone pair is active or inactive. No doubt, the problem is more complicated if some ligand has pre-defined pocket/compartment as in $[L^8]^{2-}$ in **31** and in $[L^6]^{2-}$ in **32**–**34**. Nonetheless, it is interesting to note that it has been possible to identify the stereochemically active lone pair of electrons in three (**31**–**33**) of the four title compounds and it has also been concluded that the fourth compound (**34**) has stereochemically inactive lone pair of electrons, which is clearly crucial for the drastically distorted coordination environment of lead(II) in **31**–**33** in contrast to a much less distorted geometry (distorted octahedral) in **34**.

References

(1) Desiraju, G. R. (Ed.), *The Crystal as a Supramolecular Entity*, *Perspectives in Chemistry* 2 Wiley, London, 1996.

(2) Desiraju, G. R.; Vittal, J. J.; Ramanan, *A*. *Crystal Engineering – A Texbook*, World Scientific, 2011.

(3) The Cambridge Structural Database (CSD), version 1.17, The Cambridge Crystallographic Data Center, Cambridge, UK, 2014.

(4) Mukherjee, S.; Joarder, B.; Desai, A. V.; Manna, B.; Krishna, R.; Ghosh, S. K. *Inorg*. *Chem*. **2015**, *54*, 4403.

(5) Joarder, B.; Chaudhari, A. K.; Ghosh, S. K. *Inorg*. *Chem*. **2012**, *51*, 4644.

(6) Nagarkar, S. S.; Chaudhari, A. K.; Ghosh, S. K. *Inorg*. *Chem*. **2012**, *51*, 572.

(7) Nagarkar, S. S.; Das, R.; Poddar, P.; Ghosh, S. K. *Inorg*. *Chem*. **2012**, *51*, 8317.

(8) Bose, P.; Ravikumar, I.; Ghosh, P. *Inorg*. *Chem*. **2011**, *50*, 10693.

(9) Ahamed, B. N.; Arunachalam, M.; Ghosh, P. *Inorg*. *Chem*. **2011**, *50*, 4772.

(10) Tripathy, D.; Ramkumar, V.; Chand, D. K. *Cryst*. *Growth Des*. **2013**, *13*, 3763.

(11) Niranjana, P.; Pati, A.; Porwal, S. K.; Ramkumar, V.; Gharpure, S. J.; Chand, D. K. *CrystEngComm* **2013**, *15*, 9623.

(12) Qureshi, N.; Yufit, D. S.; Steed, K. M.; Howard, J. A. K.; Steed, J. W. *CrystEngComm* **2016**, *18*, 5333.

(13) Domasevitch, K. V.; Solntsev, P. V.; Gural'skiy, I. A.; Krautscheid, H.; Rusanov, E. B.; Chernega, A. N.; Howard, J. A. K. *Dalton Trans*. **2007**, 3893.

(14) Domasevitch, K. V.; Gural'skiy, I. A.; Solntsev, P. V.; Rusanov, E. B.; Krautscheid, H.; Howard, J. A. K.; Chernega, A. N. *Dalton Trans*. **2007**, 3140.

(15) Chen, S.-S.; Fan, J.; Okamura, T.; Chen, M.-S.; Su, Z.; Sun, W.-Y.; Ueyama, N. *Cryst*. *Growth Des*. **2010**, *10*, 812.

(16) Han, Y.; Li, X.; Li, L.; Ma, C.; Shen, Z.; Song, Y.; You, X. *Inorg*. *Chem*. **2010**, *49*, 10781.

(17) Branzea, D. G.; Guerri, A.; Fabelo, O.; Ruiz-Pérez, C.; Chamoreau, L.-M.; Sangregorio, C.; Caneschi, A.; Andruh, M. *Cryst*. *Growth Des*. **2008**, *9*, 941.

(18) Thuéry, P.; Harrowfield, J. *Inorg*. *Chem*. **2016**, *55*, 6799.

(19) Batten, S. R.; Murray, K. S. *Coord*. *Chem*. *Rev*. **2003**, *246*, 103.

(20) Lin, H.-H.; Mohanta, S.; Lee, C.-J.; Wei, H.-H.; *Inorg*. *Chem*. **2003**, *42*, 1584.

(21) Misra, P.; Liao, C.-Y.; Wei, H.-H.; Mohanta, S. *Polyhedron* **2008**, *27*, 1185.

(22) Branzea, D. G.; Sorace, L.; Maxim, C.; Andruh, M.; Caneschi, A. *Inorg*. *Chem*. **2008**, *47*, 6590.

(23) Sadhukhan, D.; Ray, A.; Butcher, R. J.; Gomez-García, C. J. Dede, B.; Mitra, S. *Inorg*. *Chim*. *Acta* **2011**, *376*, 245.

(24) Sadhukhan, D.; Ray, A.; Rosair, G.; Charbonnière, L.; Mitra, S. *Bull*. *Chem*. *Soc*. *Jpn*. **2011**, *84*, 211.

(25) Shi, Q.; Sheng, L.; Ma, K.; Sun, Y.; Cai, X.; Liu, R.; Wang, S. *Inorg*. *Chem*. *Commun*. **2009**, *12*, 255.

(26) Das, L. K.; Ghosh, A. *CrystEngComm* **2013**, *15*, 9444.

(27) Mondal, S.; Mandal, S.; Jana, A.; Mohanta, S. *Inorg*. *Chim*. *Acta* **2014**, *415*, 138.

(28) Bencini, A.; Benelli, C.; Caneschi, A.; Carlin, R. L.; Dei, A.; Gatteschi, D. *J*. *Am*. *Chem*. *Soc*. **1985**, *107*, 8128.

(29) Gillon, B.; Cavata, C.; Schweiss, P.; Journaux, Y.; Kahn, O.; Schneider, D. *J*. *Am*. *Chem*. *Soc*. **1989**, *111*, 7124.

(30) Ruiz, R.; Lloret, F.; Julve, M.; Faus, J.; Muñoz, M. C.; Solans, X. *Inorg*. *Chim*. *Acta* **1993**, *213*, 261.

(31) Ercan, F.; Atakol, O.; Arici, C.; Svoboda, I.; Fuess, H. *Acta Crystallogr*., *Sect*. *C* **2002**, *58*, m193.

(32) Franceschi, F.; Solari, E.; Scopelliti, R.; Floriani, C. *Angew*. *Chem*., *Int*. *Ed*. **2000**, *39*, 1685.

(33) Thurston, J. H.; Ely, T. O.; Trahan, D.; Whitmire, K. H. *Chem*. *Mater*. **2003**, *15*, 4407.

(34) Oz, S.; Titiš, J.; Nazir, H.; Atakol, O.; Boča, R.; Svoboda, I.; Fuess, H. *Polyhedron* **2013**, *59*, 1.

(35) Mondal, S. Mandal, S.; Carrella, L.; Jana, A.; Fleck, M.; Kohn, A.; Rentschler, E.; Mohanta, S. *Inorg*. *Chem*. **2015**, *54*, 117.

(36) Mandal, L.; Bhattacharya, S.; Mohanta, S. *Inorg*. *Chim*. *Acta* **2013**, *406*, 87.

(37) Biswas, A.; Mondal, S.; Mandal, L.; Jana, A.; Chakraborty, P.; Mohanta, S. *Inorg*. *Chim*. *Acta* **2014**, *414*, 199.

(38) Costes, J.-P.; Dahan, F.; Dupuis, A.; Laurent, J.-P.; *Inorg. Chem*. **1997**, *36*, 3429.

(39) Andruh, M.; Branzea, D. G.; Gheorghe, R.; Madalan, A. M. *CrystEngComm* **2009**, *11*, 2571.

(40) Andruh, M. *Dalton Trans*. **2015**, *4*4, 16633.

(41) Cunningham, D.; McArdle, P.; Mitchell, M.; Chonchubhair, N. N.; O'Gara, M.; Franceschi, F.; Floriani, C. *Inorg. Chem*. **2000**, *39*, 1639.

(42) Majumder, S.; Koner, R.; Lemoine, P.; Nayak, M.; Ghosh, M.; Hazra, S.; Lucas, C. R.; Mohanta, S. *Eur. J. Inorg. Chem*. **2009**, 3447.

(43) Biswas, A.; Ghosh, M.; Lemoine, P.; Sarkar, S.; Hazra, S.; Mohanta, S. *Eur. J. Inorg. Chem*. **2010**, 3125.

(44) Biswas, A.; Mondal, S.; Mohanta, S. *J. Coord. Chem*. **2013**, *66*, 152.

(45) Bhattacharya, S. Jana, A.; Mohanta, S. *Polyhedron* **2013**, *62*, 234.

(46) Hazra, S.; Titiš, J.; Valigura, D.; Boča, R.; Mohanta, S. *Dalton Trans*. **2016**, *45*, 7510.

(47) Jana, A.; Mohanta, S.; *CrystEngComm* **2014**, *16*, 5494.

(48) Hazra, S.; Koner, R.; Nayak, M., Sparkes, H. A.; Howard, J. A. K.; Dutta, S.; Mohanta, S. *Eur. J. Inorg. Chem*. **2009**, 4887.

(49) Chakraborty, P.; Majumder, S.; Jana, A.; Mohanta, S. *Inorg. Chim. Acta* **2014**, *410*, 65.

(50) Hazra, S. Koner, R.; Nayak, M.; Sparkes, H. A.; Howard, J. A. K.; Mohanta, S.; *Cryst. Growth Des*. **2009**, *9*, 3603.

(51) Sasmal, S.; Majumder, S.; Hazra, S.; Sparkes, H. A.; Howard, J. A. K.; Nayak, M.; Mohanta, S.; *CrystEngComm* **2010**, *12*, 4131.

(52) Nayak, M.; Jana, A.; Fleck, M.; Hazra, S.; Mohanta, S. *CrystEngComm* **2010**, *12*, 1416.

(53) Sarkar, S.; Mohanta, S. *RSC Adv*. **2011**, *1*, 640.

(54) Mondal, S.; Hazra, S.; Sarkar, S.; Sasmal, S.; Mohanta, S. *J. Mol. Struct*. **2011**, *1004*, 204.

(55) Hazra, S.; Sasmal, S.; Nayak, M.; Sparkes, H. A.; Howard, J. A. K.; Mohanta, S. *CrystEngComm* **2010**, *12*, 470.

(56) Nayak, M.; Koner, R.; Lin, H.-H.; Florke, U.; Wei, H.-H.; Mohanta, S. *Inorg*. *Chem*. **2006**, *45*, 10764.

(57) Jana, A.; Koner, R.; Nayak, M.; Lemoine, P.; Dutta, S.; Ghosh, M.; Mohanta, S. *Inorg*. *Chim*. *Acta* **2011**, *365*, 71.

(58) Sarkar, S.; Nayak, M.; Fleck, M.; Dutta, S.; Flörke, U.; Koner, R.; Mohanta, S. *Eur*. *J*. *Chem*. **2010**, 735.

(59) Jana, A.; Koner, R.; Weyhermueller, T.; Lemoine, P.; Ghosh, M.; Mohanta, S. *Inorg*. *Chim*. *Acta* **2011**, *375*, 263.

(60) Jana, A.; Majumder, S.; Carrella, L.; Nayak, M.; Weyhermueller, T.; Dutta, S.; Rentschler, E.; Koner, R.; Mohanta, S. *Inorg*. *Chem*. **2010**, *49*, 9012.

(61) Constable, E. C.; Zhang, G.; Housecroft, C. E.; Neuburger, M.; Zampese, J. A. *Inorg*. *Chim*. *Acta* **2010**, *363*, 4207.

(62) Kurtaran, R.; Yildirim, L. T.; Azaz, A. D.; Namli, H.; Atakol, O. *J*. *Inorg*. *Biochem*. **2005**, *99*, 1937

(63) Biswas, S.; Ghosh, A. *Indian J*. *Chem*., *Sect*.*A*: *Inorg*., *Bioinorg*., *Phys*., *Theor*. *Anal*. *Chem*. **2011**, *50*, 1356.

(64) Atakol, O.; Durmus, S.; Durmus, Z.; Arici, C.; Cicek, B. *Synth*. *React*. *Inorg*. *Met*. *Org*. *Chem*. **2001**, *31*, 1689.

(65) Sari, M.; Durmus, S.; Atakol, O; Svoboda, I.; Fuess, H. *Acta Crystallogr*., *Sect*.*E* **2001**, *57*, m201.

(66) Reglinski, J.; Morris, S.; Stevenson, D. E. *Polyhedron* **2002**, *21*, 2167.

(67) Thurston, J. H.; Tang, C. G.-Z.; Trahan, D. W.; Whitmire, K. H. *Inorg*. *Chem*. **2004**, *43*, 2708.

(68) Wang, H.; Zhang, D.; Ni, Z.-H.; Li, X.; Tian, L.; Jiang, J. *Inorg*. *Chem*. **2009**, *48*, 5946.

(69) Dolai, M.; Mistri, T.; Panja, A.; Ali, M. *Inorg*. *Chim*. *Acta* **2013**, *399*, 95.

(70) Wang, H.; Zhang, D.; Tian, L.; Zhang, L.-F. *Acta Crystallogr*., *Sect*.*E* **2008**, *64*, m1460.

(71) Wang, H.; Zhang, D.; Zhang, L.-F. *Acta Crystallogr*., *Sect*.*E* **2008**, *64*, m1408.

(72) Gillespie, R. J.; Hargittai, I. *The VSEPR Model of Molecular Geometry*, Allyn and Bacon, Boston, MA, 1991.

(73) Shimoni-Livny, L.; Glusker, J. P.; Bock, C. W. *Inorg*. *Chem*. **1998**, *37*, 1853.

(74) Alizadeh, R.; Amani, V. *Struct Chem* **2011**, *22*, 1153.

(75) Morsali, A. *Z. Naturforsch*., **2004**, *59b*, 1039.

(76) Wang, S.; Mitzi, D. B.; Feild, C. A.; Guloy, A.; *J. Am. Chem. Soc*. **1995**, *117*, 5297.

(77) Elerman, Y.; Svoboda, I.; Feuss, H. *Z. Kristallogr*. **1991**, *196*, 309.

(78) Corden, J. P.; Errington, W.; Moore, P.; Wallbridge, M. G. H. *Acta Crystallogr. Sect.C*., *Cryst. Struct. Commun*. **1996**, *52*, 125.

(79)] Arici, C.; Ercan, F.; Atakol, O.; Cakirer, O. *Acta Cryst. Sec. C* **1999**, *C55*, 1654.

(80) Chen, B. H.; Yao, H. H.; Huang, W. T.; Chattopadhyay, P.;; Lo, J. M. Lu, T. H. *Solid State Sci*. **1999**, *1*, 119.

(81) Sheldrick, G. M. SAINT, Version 6.02, SADABS, Version 2.03; Bruker AXS, lnc.: Madison, WI, 2002.

(82) Sheldrick, G. M. SHELXTL, Version 6.10, Bruker AXS, lnc.: Madison, WI, 2002.

(83) Sheldrick, G. M. SHELXL-97, Crystal Structure Refinement Program; University of Göttingen: Göttingen, 1997.

(84) Lewis, D. L.; Estes, E. D.; Hodgson, D. J. *J. Cryst. Mol. Struct*. **1975**, *5*, 67.

(85) Geary, W. J. *Coord. Chem. Rev*. **1971**, *7*, 81.